

Localized HB-EGF Signaling and Connexin43 Decrease in the Myocardium

by

Robin Neely Prince

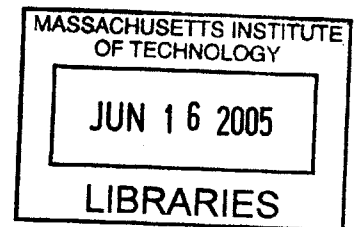
B.S., Mechanical Engineering
University of Arkansas - Fayetteville, 2003

SUBMITTED TO THE DEPARTMENT OF MECHANICAL ENGINEERING IN
PARTIAL FULFILLMENT OF THE REQUIREMENTS FOR THE DEGREE OF

MASTER OF SCIENCE IN MECHANICAL ENGINEERING
AT THE
MASSACHUSETTS INSTITUTE OF TECHNOLOGY

JUNE 2005

© 2005 Massachusetts Institute of Technology. All rights reserved.



Signature of Author: _____
Department of Mechanical Engineering
May 26, 2005

Certified by: _____
Douglas A. Lauffenburger
Director, Biological Engineering Division
Thesis Supervisor

Certified by: _____
Richard T. Lee
Associate Professor of Medicine, Harvard Medical School
Thesis Supervisor

Certified by: _____
Roger D. Kamm
Professor of Mechanical Engineering
Mechanical Engineering Thesis Reader

Accepted by: _____
Lallit Anand
Graduate Chairman
Professor of Mechanical Engineering

BARKER

Localized HB-EGF Signaling and Connexin43 Decrease in the Myocardium

by

Robin Neely Prince

Submitted to the Department of Mechanical Engineering
on May 20, 2005 in Partial Fulfillment of the Requirements for
the Degree of Master of Science in Mechanical Engineering

ABSTRACT

Growth factor signaling can affect tissue remodeling through autocrine and paracrine mechanisms. Recent evidence indicates that hypertrophic signaling in cardiomyocytes is induced through transactivation of the epidermal growth factor (EGF) receptor by heparin-binding EGF (HB-EGF). Here it is shown that HB-EGF operates in a spatially restricted local circuit in the extracellular space within the myocardium, revealing the critical nature of the local microenvironment in intercellular signaling. *In vitro* studies demonstrated that HB-EGF acts as an autocrine growth factor in cultures of rat neonatal cardiomyocytes. However, *in vivo* experiments in adult mouse left ventricles demonstrated that HB-EGF secretion by a given cardiomyocyte leads to cellular hypertrophy in cells overexpressing HB-EGF and in adjacent cells, but not in cells farther away. This highly localized microenvironment of HB-EGF signaling was also demonstrated using 3D morphology to assess cardiomyocyte growth and was predicted by a computational model of HB-EGF diffusion and binding in the myocardium. Additionally, *in vitro* and *in vivo* studies demonstrated that HB-EGF promotes loss of the principal ventricular gap junction protein Connexin43 (Cx43) in cardiomyocytes. Thus, HB-EGF acts as an autocrine and local paracrine cardiac growth factor that leads to loss of gap junction proteins within a spatially confined microenvironment within the myocardium. This demonstration of localized intercellular signaling demonstrates how cells can coordinate remodeling with their immediate neighboring cells without affecting others nearby.

Thesis Co-Supervisor: Douglas A. Lauffenburger
Title: Director, Biological Engineering Division

Thesis Co-Supervisor: Richard T. Lee
Title: Associate Professor of Medicine, Harvard Medical School

Biographical Note

I was awarded the degree of Bachelor of Science in Mechanical Engineering, Magna Cum Laude from the University of Arkansas – Fayetteville in May 2003. I enrolled in the Mechanical Engineering Department at the Massachusetts Institute of Technology in September of 2003. During my time at MIT, I have been co-supervised by Douglas A. Lauffenburger, Director of the Biological Engineering Division and Richard T. Lee, Associate Professor of Medicine, Harvard Medical School. The majority of the research presented in this master's thesis was performed in Richard Lee's lab at Brigham and Women's Hospital.

Awards

National Science Foundation (NSF) Graduate Fellow
American Association of University Women (AAUW) Selected Professions Graduate Fellow
2003 Outstanding Mechanical Engineering Senior, University of Arkansas

Professional Experience

Research Assistant, Massachusetts Institute of Technology, September 2003-present
Research Assistant, University of Arkansas, December 2000 – May 2003
NSF Research Experience for Undergraduates (REU), Microelectronics and Photonics,
University of Arkansas, May-August 2002
Lockheed Martin, Missile and Fire Control, Quality Engineering Intern, May-December 2001
International Paper, Mechanical Engineering Intern, May-August 2000

Publications

Yoshioka J, Prince RN, Huang H, Perkins SB, Cruz FU, MacGillivray C, Lauffenburger DA, Lee RT. Cardiomyocyte hypertrophy and degradation of Connexin43 through spatially restricted autocrine/paracrine HB-EGF. Submitted for publication, 2005.
Taylor C., Prince R., Malshe A., Riester L., Salamo G., Oh Cho S., Characterization of ultra-low-load (μN) nanoindentations in GaAs (100) using a cube corner tip. accepted for publication in the Journal of Smart Materials and Structures (2005).
Prince R, Taylor C, Malshe A. Study of nanoindentation and tip geometry in GaAs (100) at ultra-low-loads for the patterning of quantum dots. *Inquiry: Undergraduate Research Journal of the University of Arkansas*. 4 (2002) 101-105.
Taylor C, Prince R, Malshe A. Ultra-low-load nanoindentation in GaAs (100) for the patterning of 3-D quantum structures. *SPIE International Symposium on Smart Materials, Nano-, and Micro-Smart Systems Conference Proceedings*; Melbourne, Australia (2002).

Contents

Chapter One: Introduction

Chapter Two: Material and Methods

Chapter Three: HB-EGF adenovirus verification and *in vitro* signaling analysis

This chapter is dedicated to proving that the HB-EGF adenovirus produced in Richard T. Lee's Lab works properly, and induces hypertrophy in cultures of rat neonatal cardiomyocytes. Additionally, with this data, it can be concluded that HB-EGF acts as an autocrine growth factor *in vitro*.

Chapter Four: Computational analysis of HB-EGF signaling *in vivo*

Chapter four presents a detailed description and analysis of the computational model derived and numerically solved to predict the extent of HB-EGF diffusion in the myocardium. This model predicts that HB-EGF acts as an autocrine and localized paracrine signal.

Chapter Five: *In vivo* HB-EGF signaling analysis

This chapter focuses on HB-EGF signaling in the mouse myocardium, and illustrates that HB-EGF acts as an autocrine and local paracrine growth factor *in vivo*.

Chapter Six: Ad-HB-EGF decreases Connexin43

Chapter six is dedicated to studying the effect that HB-EGF has Connexin43 *in vivo* and *in vitro*, and illustrates that Ad-HB-EGF causes a decrease in Connexin43. This chapter also includes data and discussion which suggest that exogenous and recombinant HB-EGF may signal differently in regards to Connexin43.

Chapter Seven: Discussion

Chapter Eight: Future Directions

Chapter One: Introduction

Cell Communication

In multicellular organisms communication between cells is crucial for function and synchronization of processes. Cells respond to a variety of stimuli, including signaling molecules, heat, stress, and light. The field of mechanotransduction studies how biological systems perceive mechanical stresses and transform them into chemical signals which result in cell behavioral responses. In the cardiovascular system, proper cell communication is crucial to control the beating process and react to changes in work load.

Signaling by soluble extracellular molecules is classified by the distance in which the signal acts. Free ligands can signal in an endocrine, paracrine, or autocrine manner. Endocrine signaling molecules travel the farthest, from an endocrine organ to target cells, where the molecules typically travel through blood or extracellular fluids (Lodish 2004). However, on a much shorter length scale, **paracrine and autocrine signaling** affect cells only in close proximity. In paracrine signaling, a cell produces a soluble ligand which diffuses to and binds another cell in close proximity. Autocrine signaling differs in that the cell that produces the soluble ligand is also activated by the same ligand it produces. In this case, the cell is talking to itself in an extracellular manner. However, not all extracellular signals are diffusible. Some growth factors are active in their membrane bound form before cleavage produces the soluble factor. Juxtacrine signaling takes place when cell receptors are activated by the membrane bound ligand of an adjacent cell. Knowledge of the signaling mechanism present in a particular system gives insight to the reach and intended target of the signal.

The EGF System

The epidermal growth factor receptor (EGFR) system is a well studied example of cell communication in regards to growth, motility, and development. The EGFR family consists of four receptor tyrosine kinases: erbB1/HER1, referred to as the epidermal growth factor receptor (EGFR), erbB2/HER2, erbB3/HER3, and erbB4/HER4. Upon ligand binding, the EGF receptors dimerize and stimulate intracellular signal transduction pathways which encourage the cell to proliferate, differentiate, or survive (Lodish 2004). One well known ligand for the EGFR, epidermal growth factor (EGF), is approaching its fiftieth birthday. However, its cousin, **heparin-binding EGF** (HB-EGF), was discovered in 1991 in the medium of cultured macrophage-like cells (Higashiyama 1991). Both EGF and HB-EGF are synthesized in membrane anchored forms (pro-EGF, pro-HB-EGF) and are subsequently cleaved at an

extracellular site via a metalloprotease to release the soluble growth factor (Asakura 2002, Sahin 2004). The ability of HB-EGF and EGF to activate their corresponding receptors is not dependent on cleavage; both the pro-membrane and soluble forms can serve as cellular signals (Massague 1993).

HB-EGF has several key features which differ from EGF. HB-EGF shares the same binding domain to EGFR as EGF which consists of six conserved cysteines, however, only approximately 40% of the carboxyl portion protein sequence is homologous to EGF (Higashiyama 1991). Additionally, as its name suggests, HB-EGF binds strongly to heparin. EGF is selective for the EGFR, yet HB-EGF binds to EGFR, erbB4/HER4 (Elenius 1997), and heparan sulfate proteoglycans (Higashiyama 1993) on the cell surface. HB-EGF is an 8.3 kDa protein; however, after heavy O-glycosylation it has an estimated mass of 20-22 kDa. HB-EGF expression is present primarily in the lung, skeletal muscle, brain and heart (Abraham 1993).

Binding of ligands to receptor tyrosine kinases activate various intracellular signaling pathways. In particular, EGFR activation signals through the Ras-MAP kinase pathway. Activation of the EGFR leads to activation of the intercellular membrane bound protein, Ras. Activated Ras leads to activation of a cascade of kinases including MAP kinase, also known as ERK, Jun N-terminal Kinase (JNK), and p38, which are active in their phosphorylated form. Activated ERK dimerizes and can translocate into the nucleus to activate various transcription factors. In addition to the Ras-MAP kinase pathway, the EGFR has also been linked to the JAK-STAT pathway. JAK is a tyrosine kinase and STAT is a transcription factor, in the case of EGFR, STAT3, and STAT1 are in action. EGF binding to the EGFR also activates Akt.

Cardiac Hypertrophy

Cardiac hypertrophy occurs when individual cardiomyocytes (the beating heart cell) expand in size under excess mechanical force to increase output and therefore meet physiologic demands (Chien 1999). As a normal adaptive response mechanism, cardiac hypertrophy is not dangerous until the condition of persistent stress over time evolves into dysfunction and myocardial failure (Chien 1999). Excess mechanical load is not the only promoter of hypertrophy; others include growth factors released by stressed myocytes or other sources (non-myocytes, endocrine system, extracellular matrix, etc.).

Several extracellular signaling molecules regulate the hypertrophic response along various time courses and length scales. The endocrine systems plays a role in meeting long-term demands of the cardiovascular system through the release of growth hormone, thyroid hormone, retinoids, and vitamin D (Chien 1999). On the cellular scale for more localized cell

communication are cytokines, peptides, ligands for receptor tyrosine kinases, and heptahelical receptor agonists. The cytokines include interleukin-1, gp130-signaling cytokines, and tumor necrosis factor. The group of heptahelical receptor agonists includes angiotensin II, endothelin-1, and prostaglandin F₂ α (Chien 1999). The peptides and ligands of receptor tyrosine kinases include insulin-like growth factor-1, fibroblast growth factor, transforming growth factor beta-1, and HB-EGF.

In addition to an increase in cell size, cardiac hypertrophy is also associated with an increase in protein synthesis within cells and re-expression of fetal genes (Sadoshima 1997). The increase in protein synthesis may be required for the cell to increase in size. These embryonic genes often include atrial natriuretic peptide/factor (ANP/ANF), β -myosin heavy chain (β MHC), and skeletal α -actin (Sadoshima 1997).

HB-EGF's Role in Cardiac Hypertrophy

The pathway from HB-EGF to cardiac hypertrophy is a prime example of mechanotransduction at work. Increasing evidence suggests that stress on cardiomyocytes leads to production of endothelin-1, which induces metalloprotease cleavage of pro-HB-EGF (Anderson 2004). The soluble growth factor is then free to diffuse and activate the EGFR and subsequent intracellular signaling pathways which lead to cardiac hypertrophy (Figure 1). Evidence which supports this theory include: strain on myocytes activates the EGFR and increases the concentration of HB-EGF in cell medium (Anderson 2003), inhibition of pro-HB-EGF cleavage prevents G-protein coupled receptor (GPCR) agonist induced hypertrophy (Asakura 2002); and inhibition of NAD(P)H oxidase which leads to endothelin-1 release inhibits HB-EGF shedding (Anderson 2004). Studies suggest that ADAM12 is the metalloprotease responsible for HB-EGF shedding in the heart in relation to cardiac hypertrophy (Asakura 2002); however in mouse embryonic fibroblasts ADAM17 appears to be key (Sahin 2004).

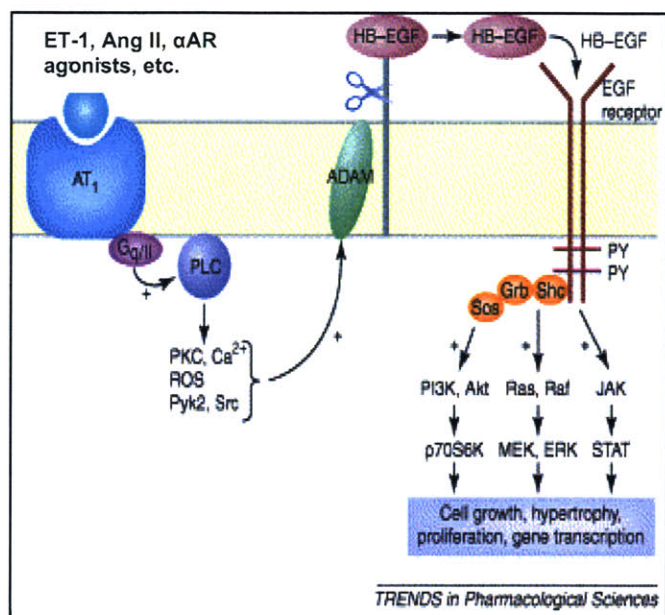


Figure 1. Current hypothesis on HB-EGF Signaling in Hypertrophy. Stress commonly leads to release of factors, such as endothelin-1 (ET-1) or angiotensin II (Ang II), which signal to G-Protein Coupled Receptors (GPCR). Activation of the GPCR, leads to cleavage of pro-HB-EGF by the metalloprotease ADAM. After EGFR activation, many intracellular signaling pathways are activated, which lead to the hypertrophic response.

Gap Junctions

Gap junctions are an important component of cell communication. These junctions connect neighboring cells and allow small molecules less than 1kDa to freely pass from the cytoplasm of one cell to the next, which is referred to as gap junctional intercellular communication (GJIC). Gap junctions in vertebrates are composed of connexins. Each connexin is composed of six connexons, which join together in the plasma membrane in a ring structure to form a hemichannel. One connexin hemichannel from a cell will dock with a hemichannel in a neighboring cell and form a channel, or gap junction. In the heart, connexon channels are crucial, allowing the rapid progression of a Ca^{+2} wave from cell to cell which simultaneously leads to the excitation and contraction of a cardiomyocyte. There are several connexin genes in vertebrates which vary in their permeability and molecular weight. **Connexin43** is the dominant gap junction in the ventricle of the heart. Large variations in the quantity of cardiomyocyte Connexin43 alter the conductance for Ca^{+2} waves throughout the heart. This can lead to loss of synchrony in myocyte contractions, referred to as a ventricular arrhythmia.

EGF & Metabolism of Connexin 43

Increasing evidence suggests that EGF affects gap junctional intercellular communication (GJIC) via Connexin43. In rat liver epithelial cells EGF and/or activation of the EGFR phosphorylates Connexin43 (Abdelmohsen 2003, Lau 1992), reduces GJIC (Lau 1992), and regulates ubiquitination, internalization and proteasome-dependent degradation of Connexin43 (Leithe 2004). Additionally, EGF down-regulates Connexin43 expression in rat cortical astrocytes (Ueki 2001). The mechanism of EGF induced Connexin43 phosphorylation may lie in the MAP kinase pathway after activation of the EGFR (Warn-Cramer 1998, Rivedal 2001). Phosphorylation of the MAP kinase member, JNK, leads to a decrease in Connexin43 in cardiomyocytes (Petrich 2002). In contrast, in cultures of granulosa cells from preantral rabbit follicles, Connexin43 expression is increased (Bolamba 2002). However, opposing studies show that stretching and vascular endothelial growth factor (VEGF) increase connexin43 in cultures of ventricular myocytes, even though stretching is expected to produce HB-EGF in cardiomyocytes.

A reduction in Connexin43 is not only associated with the EGF pathway, but is also present in cardiac hypertrophy. Reduced content of Connexin43 is commonly observed in chronic heart diseases such as hypertrophy, myocardial infarction, and failure (Peters 1996, Kostin 2003). Hypertrophy is associated with an increased risk of cardiovascular morbidity and mortality, much of which stems from electrical remodeling and arrhythmogenesis (Volders 1998).

Remodeling

Mechanical forces in the heart lead to structural remodeling of the tissue. All components of the myocardium, from the extracellular matrix, to the adhesion proteins, to the cell itself must adjust in the presence of excess mechanical stress until a new equilibrium is achieved. Additionally, as one could imagine, remodeling may be required during hypertrophy as a cell expands in size. Gap junctions not only transfer small molecules between cells, but hold cells together, and their removal and/or repositioning may be required for a cell to hypertrophy. Locally-produced HB-EGF may travel through the extracellular space and be recaptured by the EGF receptor close to the point where it was released from the cell surface (Lauffenburger 1998, Shvartsman 2001). The impact of a spatially localized microenvironment of cell signaling, possibly caused by an unequal stress distribution, could lead to heterogeneous tissue remodeling.

Hypothesis

The objective of this study is to elucidate the signaling mechanism of HB-EGF in the heart. This study is not intended to focus on the effects of cardiac hypertrophy, but rather utilizes the

hypertrophic response as an assay to determine the extent of cell signaling. It was hypothesized that HB-EGF signals produced by cardiomyocytes operate in a spatially restricted area in the extracellular space. Also hypothesized was that HB-EGF secretion by a given cardiomyocyte could create a local remodeling microenvironment of decreased Connexin43 within the myocardium. To explore whether HB-EGF signaling is confined to a microenvironment, non-uniform gene transfer was utilized in cardiac myocytes *in vitro* and *in vivo*, as well as computational modeling to predict HB-EGF dynamics.

Chapter Two: Methods and Materials

This research was a team project, and would not have been possible without the contributions and expertise of Jun Yoshioka, Scott Perkins, Cathy MacGillivray, Francisco Cruz, Hayden Huang, and Mihaela Cupesi. In order to give others due credit for their work, I have outlined below methods that are specific to my contributions to this project, and a separate section for the methods relevant to contributions from others.

Methods Specific to My Contribution

HB-EGF Adenovirus Production

Recombinant adenoviruses are an efficient way of inserting a particular gene of interest into cells. Adenoviruses have a higher infection efficiency when compared to the alternate method of plasmid transfection. A recombinant adenovirus for the overexpression of HB-EGF and co-expression of green fluorescent protein (GFP) was produced using the AdEasy Adenoviral Vector System from Stratagene. The core virus is the human adenovirus serotype 5, which is replication defective through the deletion of the E1 and E3 genes (Stratagene 7). Murine HB-EGF cDNA was amplified using 5'-ATATATACTAGTATATGAAGCTGCTGCCGTC-3' sense and 5'-ATATATCTCGAGTCAGTGGGAGCTAGCC-3' antisense primers including SpeI and NcoI restriction sites, respectively. The PCR product was subcloned into the pShuttle-IRES-hrGFP-1 vector between SpeI and NcoI sites and sequenced to confirm that the clones corresponded to the HB-EGF (GenBank accession number NM_010415). After a recombinant was identified, it was produced in the XL10-Gold strain. Purified recombinant adenovirus plasmid DNA was digested with PAC I to expose inverted terminal repeats and then was transfected into HEK 293 cells. HEK 293 cells were lysed releasing virus into the supernatant with four cycles of freezing, thawing, and vortexing. After centrifuging at 7000g, the supernatant was transferred to an ultracentrifuge in a cesium chloride (CsCl) solution to spin at 32,000rpm at 10°C for 18-24 hours. Virus band was collected and mixed with an equal volume of adenovirus storage buffer (2x Storage Buffer: 10mM Tris, pH 8.0, 100nM NaCl, 0.1% BSA, and 50% glycerol). All viral stocks were stored at -80°C. For controls, we used the identical virus vector expressing GFP alone (Ad-GFP).

The virus was originally made by Scott B. Perkins, Richard T. Lee Lab, Brigham and Women's Hospital. Virus replication and purification was performed by myself and Jun Yoshioka.

Rat Neonatal Cardiomyocyte Cell Culture

Hearts were removed from Sprague-Dawley rat pups (1-3 days old) and washed with Hanks Buffered Saline Solution without calcium or magnesium (HBSS-). Atria was removed and hearts were finely minced and placed into a trypsin solution (1mg trypsin power / 1 mL HBSS-) for 3 hours. Hearts were digested with collagenase (0.8 mg collagenase / 1 mL HBSS-), then centrifuged at 800rpm for 5 minutes to remove the collagenase solution. Cells were cultured on dishes coated with 0.1% gelatin in PBS then grown with Dulbecco's Modified Eagle Medium (DMEM) with 7% fetal bovine serum (FBS) and a 1% penicillin/streptomycin solution. Serum starve media consisted of DMEM with 1x ITS and 1% penicillin/streptomycin solution.

Western Blotting

Equal amounts of protein were subjected to western blot analysis using the indicated antibodies: EGFR (Santa Cruz), phospho-EGFR (Santa Cruz Biotechnology), STAT3 (Cell Signaling), phospho-STAT3 (Cell Signaling), JNK (Cell Signaling), phospho-JNK (Cell Signaling), ERK1/2 (Cell Signaling), phospho-ERK1/2 (Cell Signaling), Connexin43 (Sigma), N-Cadherin (Santa Cruz Biotechnology and Sigma), ErbB4 (Santa Cruz Biotechnology), actin (Sigma), and ubiquitin (Santa Cruz Biotechnology). Additional reagents used in western blotting include recombinant human HB-EGF (Sigma and R&D Systems), recombinant human EGF (Sigma), and AG-1478 (CalBiochem)

Western Blots were performed by myself and Jun Yoshioka.

Immunoprecipitation

Cells lysates were incubated with the primary antibody, then with protein G agarose beads (Upstate). The bead-lysate mixture was centrifuged and washed 5x. The protein was then removed from the beads with buffer and subsequent boiling. The samples were subsequently analyzed with western blotting.

Immunoprecipitation was performed by myself and Jun Yoshioka.

2D Cell Cross-sectional Area Measurements *In Vivo* and *In Vitro*

Cell cross-sectional area was measured *in vivo* with a program written by Jeremy Sylvan, Brigham and Women's Hospital, Richard Lee Lab in Matlab, which allows the user to outline a cell in cross-sections of the mouse myocardium, and measure the area. This information is then exported to Microsoft Excel. Cell area was measured in a similar matter for *in vitro* studies, except that the area measured is the projected area onto the dish, rather than cross-sectional area.

Confocal Microscopy

Confocal images were taken with a Carl Zeiss LSM510 Confocal Microscope (40× and 100x). All images were taken in a blind manner with no knowledge of slide identify.

Connexin43 and Cadherin Quantification

Positive Connexin43 and N-cadherin staining per tissue area were quantified for green areas (virus infected), adjacent areas, and remote areas from confocal images. A program was written to identify green areas within an image, measure this area, and identify and quantify positive Connexin43 or N-cadherin staining with Cy5 within the green areas and a few microns around it. The program additionally analyzed and quantified Connexin43 in areas adjacent to green cells. This was performed by drawing an 18 μm radius stress around the identified green area with the strel tool, and quantifying Connexin43 in the radial areas. An additional program was written to analyze and quantify Connexin43 and N-cadherin in areas of the heart with no GFP expression, far from the site of virus injection or infection, referred to as remote areas. This program quantified positive Connexin43 and N-cadherin staining per tissue area in a box drawn in by the user. Data from each heart was normalized with Connexin 43/N-cadherin staining per remote area data to account for variations in the heart fixation conditions. All data was analyzed in a blind manner.

Mathematical Modeling

Model equations were solved numerically in Femlab 3 (Comsol) subject to boundary conditions and the defined tissue geometry. Femlab utilizes the finite element methods with an adaptive triangular mesh. The mesh had 7,633 elements, 19,433 degree of freedom, 4,229 boundary elements, with a minimum element quality of 0.6124. All computations assume the system has reached a steady state.

Statistical Analysis

All data are presented as mean+SEM. Statistical analysis was performed with the two-tailed unpaired Student's t test, Mann-Whitney rank sum test, or one-way ANOVA for multiple comparisons with the Tukey-Kramer method. Statistical significance was achieved when $P < 0.05$. *Statistical analysis was performed with the help of Jun Yoshioka.*

Methods Specific to Contributions from Others

Left Ventricle Injection of Adenovirus

Evaluation of the functional effects of a gene on cardiomyocyte growth in vivo was performed by comparing cells overexpressing the gene with cells that do not overexpress the gene in the same heart. Briefly, male FVB mice (age 10 to 12 weeks) were anesthetized with pentobarbital (30 $\mu\text{g/g}$ intraperitoneally) and adenoviral vectors (Ad-GFP or Ad-HB-EGF) were directly injected into the left ventricular free walls (2×10^9 pfu in 50 μl). At seven days following surgery, mouse hearts were harvested and fixed with 4% paraformaldehyde. All surgeries were performed in a blinded, randomized manner with respect to treatment. The Harvard Medical School Standing Committee on Animal Research approved the study protocols.

This work was completed by Mihaela Cupesi, Richard T. Lee Lab, Brigham and Women's Hospital

3D Cell Volume Measurements

Mouse hearts were labeled using a Texas Red-maleimide (Molecular Probes, Inc) tail-vein injection, followed by removing the heart, fixing with 4% paraformaldehyde and embedding in paraffin. Five micron slices were cut and plated on glass slides for a total of 200 slices. Every other slice was imaged at 10 \times using an Olympus IX70 inverted fluorescence microscope using both red (ex545/15 and em620/30) and green (ex480/20 and em535/25) filter sets to image the maleimide staining and detect the presence of GFP in the cells. Post-processing was performed first by aligning images based on identical physical features in successive slices, extracting single myocytes using the maleimide stain as the borders of the cells, and then adding the successive cross-sectional areas and multiplying by the spacing between slices (10 μm since every other slice was omitted) to obtain the cell volume. Post-processing was performed blinded to virus type in order to avoid bias.

This method was invented by and measurements were completed by Francisco U. Cruz and Hayden Huang, Richard T. Lee Lab, Brigham and Women's Hospital. Heart fixation and staining was done by Cathy MacGillivray, Richard T. Lee Lab, Brigham and Women's Hospital.

Immunohistochemistry

Paraffin-mounted histologic sections were stained with the indicated primary antibodies (1:200 to 1:50) followed by secondary antibody (1:200) conjugated with Cy3, Alexa Fluor 647, 680, or 694 (Molecular Probes, Inc).

Whole heart staining was performed by Cathy MacGillivray, Richard T. Lee Lab, Brigham and Women's Hospital.

Northern Analysis

Total RNA was isolated from cardiomyocytes by the guanidinium thiocyanate and phenol chloroform method using TRI reagent (Sigma). For Northern blotting, 15 µg of total RNA was loaded on a 1.0% formaldehyde gel (2.0 M), transferred to a nylon membrane (Stratagene), and UV cross-linked with a UV Stratalinker (Stratagene). The cDNA fragment corresponding to rat Connexin43 (GenBank accession number NM 012567) was radiolabeled by the random priming method with [³²P]dCTP and the Klenow fragment of DNA polymerase (Stratagene). This radiolabeled probe was hybridized on the membrane with QuikHyb solution (Stratagene) at 68C for 1 h. The membrane was exposed to x-ray film overnight at 80C with one intensifying screen. Normalization of RNA for equal loading was carried out by hybridizing the blots with a glyceraldehyde-3-phosphate dehydrogenase (GAPDH) cDNA probe (CLONTECH, Palo Alto, CA). Levels of Connexin43 and GAPDH mRNA were quantified by densitometry of the Northern blot autoradiographs using Scion Image software (version 4.02; Scion Corp.).

This work was completed by Jun Yoshioka, Richard T. Lee Lab, Brigham and Women's Hospital

Leucine Incorporation

Protein synthesis in neonatal rat cardiomyocytes was quantified by [³H]Leucine (New England Nuclear-Life Science Products, Boston, MA) incorporation. Cells were infected with Ad-GFP or ad-HB-EGF for 48 hr and then incubated in fresh DMEM containing ITS with 1.0 µCi/mL [³H]leucine for an additional 24 hr. The medium was aspirated, and the cells were washed twice with ice-cold PBS, twice with 10% trichloroacetic acid (TCA; Sigma) and fixed for 45 minutes at 4C with 10% TCA. After washings twice with 10% TCA, the radioactivity incorporated into the TCA-precipitable material was determined by liquid scintillation counting (Beckman Coulter LS6500) after solubilization in 0.15 N NaOH.

This work was completed by Jun Yoshioka, Richard T. Lee Lab, Brigham and Women's Hospital

Flow Cytometry

Forward light scattering was measured by flow cytometry, which gives an index of cell size.

Forward angle light scatter data were obtained on a Cytomics™ FC500 flow cytometer (Beckman Coulter, Fullerton, CA). The sub-G1-population of apoptotic cells was excluded by staining with propidium iodide (Sigma). Mean channel number was analyzed for 5,000 cells on the forward scatter events to give an indication of cell size.

This work was completed by Jun Yoshioka, Richard T. Lee Lab, Brigham and Women's Hospital

Chapter Three: HB-EGF adenovirus verification and *in vitro* signaling analysis

Gene transfer in cardiomyocytes was achieved with the use of adenoviral vectors expressing Green Fluorescent Protein (GFP) alone (Ad-GFP) and HB-EGF along with GFP (Ad-HB-EGF). After production of the HB-EGF/GFP expressing adenovirus, it was necessary to confirm that the virus worked properly and produced HB-EGF in significant amounts. To begin, the amount of HB-EGF produced by Ad-HB-EGF was analyzed in comparison to that produced by Ad-GFP. The western blot in Figure 2A shows that cell lysates from cardiomyocytes infected with Ad-HB-EGF cell had a much higher level of HB-EGF expression compared to Ad-GFP. However, HB-EGF was immunoprecipitated from the cell culture medium, and amounts were equal from Ad-HB-EGF and Ad-GFP infected cardiomyocytes. This suggests that Ad-HB-EGF produces a large amount of HB-EGF which remains on the cell surface, either in the pro-membrane form or possibly bound to proteoglycans and/or EGF receptors, but is not released into the culture medium. Therefore, the equal bands in the western blot of Figure 2B most likely represent basal levels of HB-EGF secretion from cardiomyocytes.

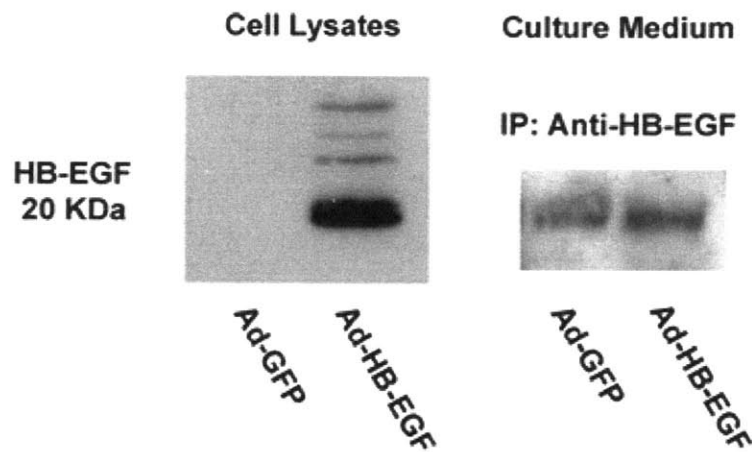


Figure 2. HB-EGF is present in Ad-HB-EGF lysates. (A) Cultured cardiomyocyte cell lysates infected with Ad-HB-EGF show much higher HB-EGF expression when compared to Ad-GFP lysates. (B) Culture medium from cardiomyocytes infected with Ad-HB-EGF and Ad-GFP had equal amounts of HB-EGF.

After confirming that Ad-HB-EGF successfully produced HB-EGF, it was necessary to confirm that the adenovirus induced cardiac hypertrophy in rat neonatal cardiomyocytes. As mentioned previously, cardiac hypertrophy is characterized by an increase in cell size, an increase in protein uptake, and reactivation of the fetal gene program (Chien 1999, Sadoshima 1997). The

first measure of hypertrophy we performed was a cell size comparison by flow cytometry and two-dimensional cell area. Evaluation of cell size over time illustrated that at four days post incubation with Ad-HB-EGF, cardiomyocytes began to hypertrophy significantly more than Ad-GFP and non-infected cells, therefore all measurements were done at three or more days post virus-infection (Figure 3A). In a 2D cell area and flow cytometry analysis, Ad-HB-EGF cells were significantly larger than Ad-GFP and non-infected cardiomyocytes *in vitro* (Figure 3B, 3C). The significant size increase in Ad-HB-EGF cardiomyocytes hinted that the HB-EGF adenovirus was successfully inducing cardiac hypertrophy. Additionally, non-infected cells on the same dish as infected cells showed no change in size in the flow cytometry analysis. This evidence demonstrates that HB-EGF signaling *in vitro* is autocrine only, and HB-EGF does not signal to neighboring cells.

Leucine incorporation is a method of measuring the amount of protein uptake of a particular cell. It has been shown previously that myocytes in the state of hypertrophy have a significant increase in leucine uptake, presumably for the production of additional proteins to increase cell size. Radiolabeled leucine incorporation was measured for cultured neonatal cardiomyocytes *in vitro* infected with Ad-HB-EGF and Ad-GFP with an amount so that the number of GFP positive cells was approximately 100% (Figure 4). Additionally, conditioned media from Ad-HB-EGF and Ad-GFP cells was removed and placed onto non-infected cardiomyocytes. The Ad-HB-EGF infected cardiomyocytes showed a significant increase in leucine incorporation over GFP expressing cells. Additionally, conditioned media from the Ad-HB-EGF infected cells produced an insignificant increase in leucine incorporation for non-infected cells relative to conditioned medium from Ad-GFP infected cells. Due to the equal levels of HB-EGF present in Figure 2B, one would expect the leucine incorporation value for Ad-GFP and Ad-HB-EGF conditioned medium to be equal. Overall, this serves as additional evidence that HB-EGF adenovirus leads to hypertrophy of infected cells.

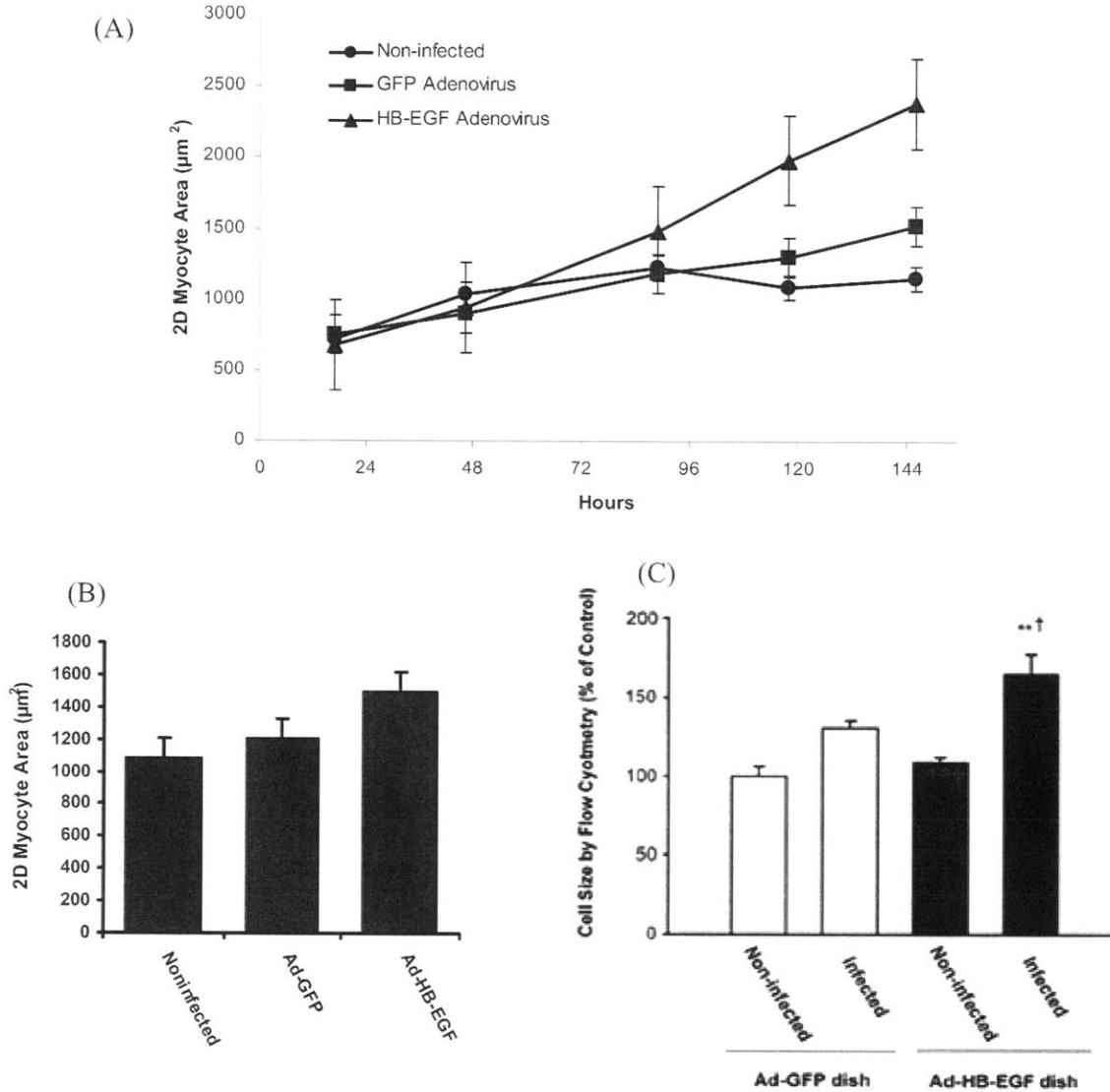


Figure 3. Cell size data confirms that Ad-HB-EGF induces size increase. (A) Cell size of cultures cardiomyocytes over time with Ad-GFP, Ad-HB-EGF, or non-infected, measured by 2D area (B) Cell size of cultures of cardiomyocytes after three plus days infected with Ad-GFP (n=72), Ad-HB-EGF (n=58), or non-infected (n=73) measured by 2D area. Ad-HB-EGF induced a 37% and 24% 2D area increase over non-infected (**P<0.01) and Ad-GFP cells (†P<0.05), respectively. (C) Cell size measured by flow cytometry (n=5,000), the adenovirus did not infect 100% of the cells per dish, therefore non-infected cells represent those without the adenovirus in the same dish as the Ad-GFP or Ad-HB-EGF cells. Ad-HB-EGF cells were 26% larger than Ad-GFP (†P<0.05), and also significantly larger than non-infected cells in the Ad-HB-EGF dish (**P<0.01).

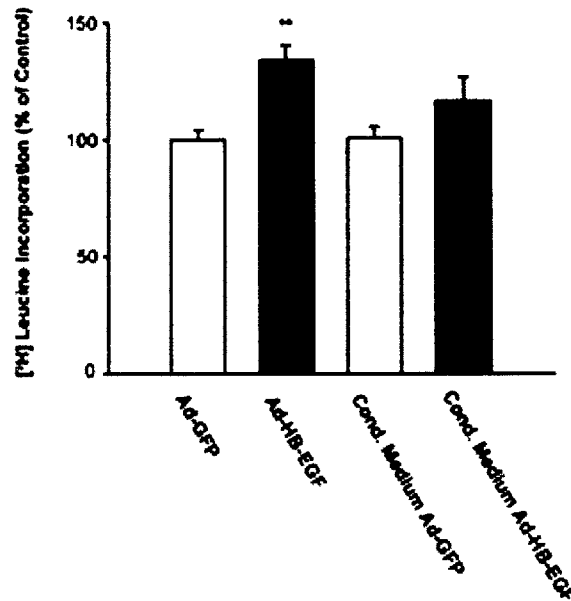


Figure 4. Protein synthesis measured by [³H] leucine incorporation illustrates that Ad-HB-EGF induces hypertrophy. Ad-HB-EGF caused cardiomyocytes to have a significant increase in leucine incorporation (34% increase, n=6, **P<0.01) over Ad-GFP cells. Additionally, medium from the virus infected cells was removed and placed on non-infected cardiomyocytes, and conditioned medium from Ad-HB-EGF plates caused an insignificant increase in leucine incorporation

After demonstrating that Ad-HB-EGF leads to the hypertrophic characteristics of an increase in cell size and protein synthesis, the next logical step was to test activation of the fetal gene program. However, results from an RT-PCR analysis from Ad-HB-EGF and Ad-GFP infected cells gave inconclusive data on ANP and β MHC gene expression (data not shown).

Next, we wanted to confirm that cardiomyocyte hypertrophy was initiated through activation of the EGFR. Therefore, phosphorylation of EGFR, phosphorylation of ERK 1/2, phosphorylation of STAT3, phosphorylation of Akt, and phosphorylation of JNK in cell lysates infected with Ad-HB-EGF and Ad-GFP was analyzed, all of which are downstream components of EGFR activation which are associated with hypertrophy. To directly observe activation of the EGFR by HB-EGF, a western blot of protein lysates from Ad-HB-EGF, Ad-GFP, and non-infected cells was probed for presence of the EGFR, and the phosphorylated, or activated, form of the EGFR. Unfortunately, after many attempts, this experiment was unsuccessful in detecting the EGF receptor in cultures of neonatal cardiomyocytes, which has been previously reported successful (Asakura 2002) (Figure 5). This suggests that the EGFR density on the surface of cardiomyocytes may be extremely low compared to that of smooth muscle cells (SMC). HB-

EGF binds not only to the EGFR, but to ErbB4 in addition. However, western blotting for the ErbB4 receptor was also unsuccessful in cultures of neonatal cardiomyocytes (data not shown).

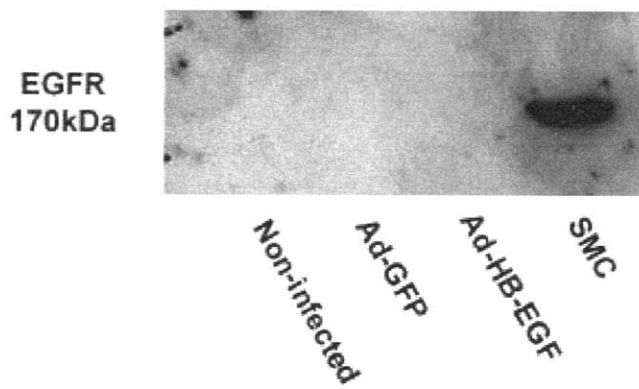


Figure 5. EGFR in cardiomyocytes. The EGF receptor could not be detected in western blots from cardiomyocytes to probe for EGFR activation. Smooth muscle cells (SMC) are used as a positive control to confirm the anti-EGFR is working properly.

EGFR activation was successfully demonstrated through indirect measurement of the downstream molecules phospho-JNK and phospho-ERK1/2 (Figure 6C, 6D). Additionally, the EGFR downstream signaling molecules, STAT3 and Akt were analyzed, and no significant change in the amount of phospho-STAT3 or phospho-Akt was present in Ad-HB-EGF lysates over Ad-GFP lysates (Figure 6A, 6B). However, for both proteins, the phosphorylated forms were detected in cell lysates of both Ad-GFP and Ad-HB-EGF in equal amounts. This differs from activated ERK1/2 and JNK, in that the phosphorylated form is only present in Ad-HB-EGF lysates. Activation of Akt in both Ad-GFP and Ad-HB-EGF is most likely due to the adenovirus protein, E4, which is present in both viruses and has been shown to phosphorylate Akt in endothelial cells (Zhang 2004). E4 may also be responsible for phosphorylation of STAT3, however this has not been reported. Additionally, activation of Akt is associated with cardiac hypertrophy (Miyamoto 2004), which may explain the insignificant increase in size and leucine incorporation of Ad-GFP cells compared to those that are non-infected.

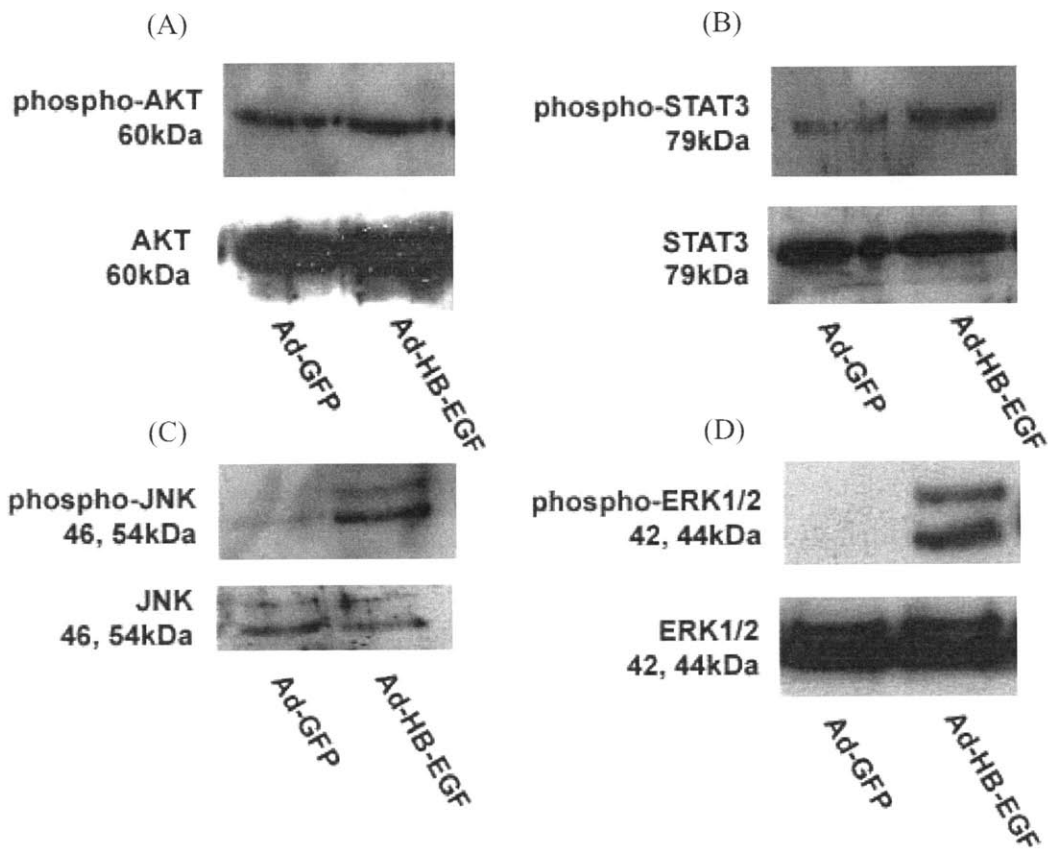
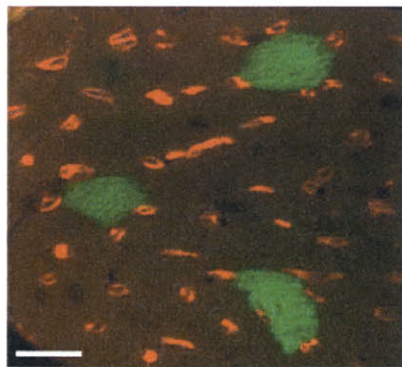


Figure 6. Activation of downstream components of the EGFR (A) Western blot of Akt in Ad-GFP and Ad-HB-EGF cells lysates show equal amounts of protein for total Akt, and equal amounts of phosphor-Akt (B) Western blot of STAT3 in Ad-GFP and Ad-HB-EGF cell lysates show equal amounts of STAT3 and phospho-STAT3 (C) Western blot of JNK in Ad-GFP and Ad-HB-EGF cells lysates show equal amounts of total JNK, but phospho-JNK is present in much higher amounts in Ad-HB-EGF cells (D) Western blot of ERK1/2 in Ad-GFP and Ad-HB-EGF cell lysates show equal amounts of total ERK1/2, but phosphor-ERK1/2 is present in much higher amounts in Ad-HB-EGF cells.

In conclusion, HB-EGF acts as an autocrine growth factor *in vitro*. The adenovirus for HB-EGF successfully produces HB-EGF and leads to hypertrophy in cultures of cardiomyocytes demonstrated by leucine incorporation and cell size. Data suggests that Ad-HB-EGF leads to hypertrophy through activation of the Ras-MAP kinase intracellular signaling pathway.

Chapter Four: Computational analysis of HB-EGF signaling *in vivo*

Although the data presented in Chapter Three showed HB-EGF as a predominantly autocrine cardiac growth factor *in vitro*, HB-EGF signaling *in vivo* takes place in a very different environment. Therefore, I sought to determine the extent that soluble HB-EGF may travel in the interstitial space of the myocardium to estimate the primary signaling mechanism. To explore this, I first designed a simple 2D model of HB-EGF diffusion within myocardium. The geometry of model was based on the geometry of the mouse myocardium, with approximately four capillaries surrounding each myocytes (Tagarakis 2000) in a square array. However, it should be noted that a hexagonal distribution of capillaries is widely accepted, which also has four capillaries surrounding each myocyte. However, I expect this simpler construction will not affect the results. Figure 7 is slice of the mouse heart which had been injected with Ad-GFP or Ad-HB-EGF. To be noted is the fact that multiple capillaries (in red) surround each myocyte in the tissue. To reflect these features in the model geometry, I chose the approximate geometric representation of myocytes in cross-section as a square ($15 \times 15 \mu\text{m}$), with each of the corners occupied by a capillary (diameter $5 \mu\text{m}$). The cell shape was chosen so that the extracellular matrix width ($0.5 \mu\text{m}$), in which soluble HB-EGF is free to diffuse, was constant around all tissue features (Figure 8B). In this 2D analysis, myocytes and capillaries are modeled as infinite in length, reflecting the long rod-like dimensions of a cardiomyocyte (Figure 8A).



Green: Infected Cells, Red: Isolectin

Figure 7. Tissue geometry of the mouse myocardium. A Mouse left ventricle cross-sections was injected with Ad-HB-EGF or Ad-GFP (green cells), and isolectin staining in red for capillaries illustrates that each myocyte is surrounded by multiple capillaries. Scale bar represents $20\mu\text{m}$.

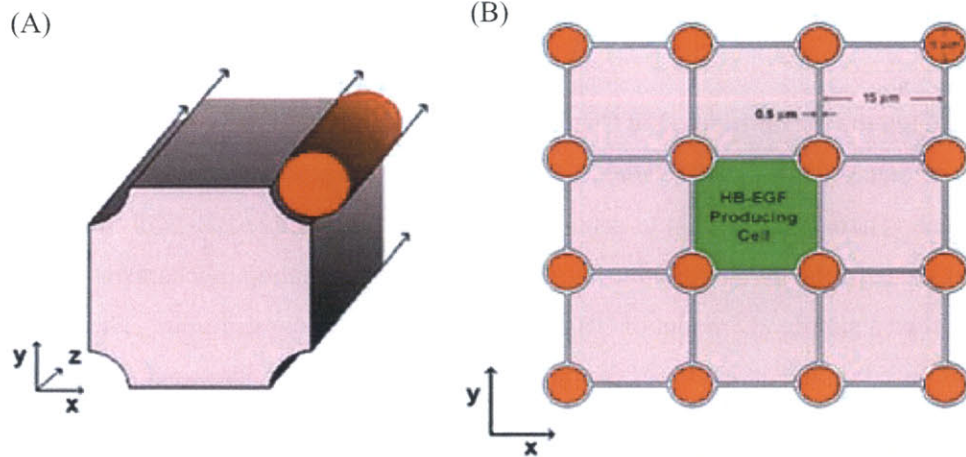


Figure 8. The Model Geometry. (A) Illustrates that due to the 2D computational analysis, cardiomyocytes and capillaries are modeled as infinite in length. (B) The model geometry with a central cell producing HB-EGF where green is HB-EGF producing cells, pink is neighboring cells, red is capillaries, and white is the extracellular space where soluble HB-EGF is free to diffuse.

The model represents a single central cell that is producing soluble HB-EGF at a constant rate (R_{gen}) and releasing it into the extracellular space. The generation rate is estimated to be on the order of magnitude of the HB-EGF concentration measured in the conditioned media, and this value is approximated at 10 \#/(cell*s) . The HB-EGF ligand is then free to diffuse throughout the extracellular space, or may enter a capillary and leave the system (Figure 9A).

The fate of HB-EGF in this mathematical system is governed by four differential equations listed below. The governing equation for ligand concentration within the extracellular space is the diffusion equation at steady state (equation 1), while equation (2) is the flux matching boundary condition for the ligand producing cell, (3) is the flux matching boundary condition for the neighboring cell, and (4) is the flux matching boundary condition at the capillaries. All equations assume a steady state.

$$\frac{\partial C}{\partial t} = D_L \nabla^2 C = 0 \quad (1)$$

$$-D \nabla C = R_{gen} \quad (2)$$

$$-D \nabla C = 0 \quad (3)$$

$$-D \nabla C = -h(C - C_{blood}) \quad (4)$$

C is the concentration of free HB-EGF, D is the diffusion constant for HB-EGF, h is the mass transfer coefficient of HB-EGF through the capillary walls, and C_{blood} is the concentration of HB-EGF in the blood, approximated to be zero.

The numerical solution at steady state is shown in Figure 9B, which illustrates that HB-EGF remains localized around the cell which produced it, and HB-EGF does not diffuse any farther due to the sink-like effect of the capillaries.

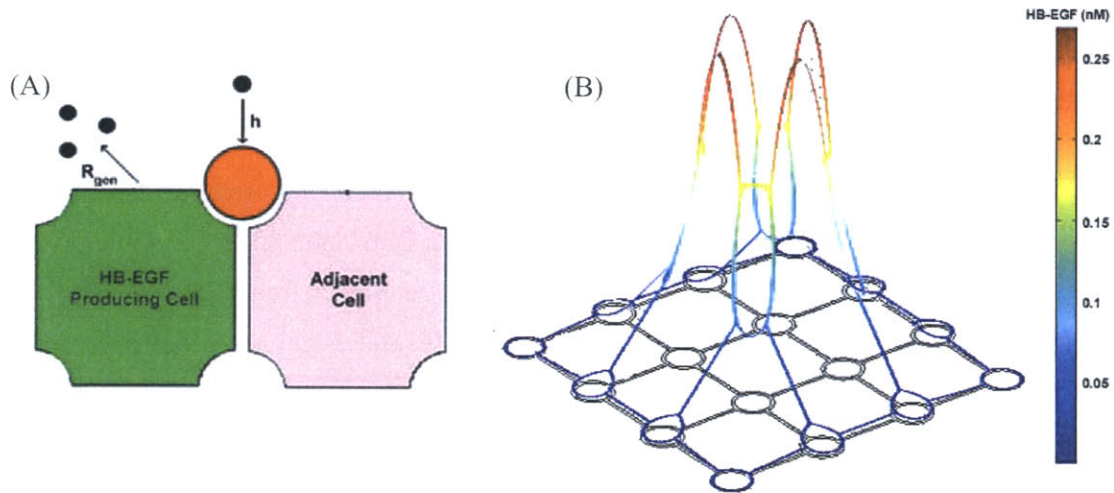


Figure 9. Molecular mechanisms and Numerical Solution of HB-EGF dynamics. (A) HB-EGF is generated by the ligand producing cell at a constant rate, R_{gen} , and is then free to diffuse throughout the extracellular space or enter the capillaries with a transport coefficient, h , and leave the system. (B) Steady state HB-EGF concentration profile predicted at base values for the parameters (see Table 1). HB-EGF concentration is shown by the color scale and height depicted. The maximum concentration achieved with the base value parameters is 0.27 nM farthest from a capillary.

The maximum concentration of soluble HB-EGF achieved is 0.27 nM, which is approximately equal to the threshold level of HB-EGF measured to stimulate cardiomyocyte growth with recombinant HB-EGF (2000 pg/mL, data not shown). Therefore, the central HB-EGF producing cell only signals to its four adjacent neighbors where the HB-EGF concentration reaches this threshold. However, if the model geometry is altered to reflect a 50% and 150% increase in cross-sectional area in all cells due to hypertrophy, approximated from one and four weeks of transverse aortic constriction, (Yoshioka 2004),(Lindsey 2003), the maximum concentration achieved increases slightly to 0.29 nM and 0.37 nM, respectively. As the dimensions of the cell increase, HB-EGF must diffuse farther to reach a capillary and therefore a higher concentration is achieved at steady state in the extracellular space. Therefore, cells adjacent to the HB-EGF producing cell are exposed to a higher concentration of HB-EGF during hypertrophy; however, the length scale in terms of the number of cells for which HB-EGF diffuses stays the same.

Perturbation of the model parameters revealed the driving forces that determine the extent to which HB-EGF travels are the rate of HB-EGF transfer into the capillaries and the diffusivity of HB-EGF. The exact mechanism of macromolecule transport into capillaries is unknown (Rippe 2002), however it is most likely through diffusion, transcytosis, or a combination of the two. In the case of diffusion, the mass transfer coefficient governing the flux of HB-EGF through the capillary wall is coupled to the diffusivity of HB-EGF, while the terms are uncoupled for the case of transcytosis. Therefore, this model assessed transcytosis as a conservative scenario for HB-EGF localization. Parameter perturbation with uncoupled diffusion and capillary mass transfer showed that HB-EGF remains localized around the origin of production and diffuses only to immediate neighbors for mass transfer coefficients greater than $0.002 \mu\text{m/s}$. For values lower than $0.002 \mu\text{m/s}$, HB-EGF diffused distances greater than two cells away from the origin. The actual mass transfer coefficient of ligands in the size range of HB-EGF is unknown, however values for O_2 ($0.02 \mu\text{m/s}$, 0.032 kDa) (Sharan 2002) and LDL ($1.7 \times 10^{-5} \mu\text{m/s}$, $2000\text{-}3000 \text{ kDa}$) (Tompkins 1991) have been reported, and we assumed HB-EGF is in the upper end of that range due to its small size. At a diffusivity of $0.7 \mu\text{m}^2/\text{s}$ (Dowd 1999), HB-EGF traveled only one cell away. However, if the diffusivity is increased to $51.8 \mu\text{m}^2/\text{s}$ (Thorne 2004), HB-EGF travels five cells away. Changing the generation rate of HB-EGF, R_{gen} , only varies the peak concentration achieved between cells. Thus, the computational model predicts that HB-EGF acts as a highly localized autocrine and paracrine growth factor within the myocardium. Parameter values and perturbation ranges can be found in Table 1.

This model of HB-EGF diffusion ignores binding of HB-EGF to the EGF receptor, heparan sulfate proteoglycans, and the extracellular matrix. EGF receptor binding and internalization would only serve to further localize the HB-EGF signal, therefore the results above are a maximum value estimate. Extracellular binding of HB-EGF does not affect the steady state concentration profile if the binding is reversible. However, matrix and proteoglycan binding could serve to slow the approach to steady state as the cell begins to produce HB-EGF, or serve as a source of HB-EGF as the cell slows or stops ligand production.

In conclusion, the computational model supports the hypothesis that HB-EGF may act as a localized signal within the myocardium due to diffusion of HB-EGF into the capillaries. However, further experimental analysis discussed in Chapter Five is needed to support this hypothesis.

Symbol	Parameter	Units	Base Value	Perturbation	Max [L] (nM)	Ref
R_{gen}	sHB-EGF Production Rate	$cell^{-1} s^{-1}$	10	1-100	0.03-2.7	(Dewitt 2004) [*]
D	HB-EGF Diffusivity	$\mu m^2 s^{-1}$	0.7	0.7^{\ddagger} -51.8 [‡]	0.02-0.27	(Dowd 1999) [†] (Thorne 2004) [‡]
h	capillary mass transfer coefficient	$\mu m s^{-1}$	0.02	0.0002-0.02	0.3-2.0	
SA	cell surface area	μm^2	5600	--	--	

^{*}EGF in engineered mouse B82 fibroblasts

[†]free bFGF in Descemet's membrane

[‡]EGF in rat brain extracellular space

Table 1. Base value estimations for the modeling parameters with their perturbation range and affect on the maximum HB-EGF concentration achieved in the system. Perturbations were performed by fixing all parameters at the base value and only varying the indicated value.

Chapter Five: *In vivo* HB-EGF signaling analysis

As presented in Chapter Three, we found the HB-EGF signaling mechanism *in vitro* in neonatal rat cardiomyocytes is autocrine only. However, HB-EGF signaling in the adult mouse myocardium takes place in a very different environment. The heart is beating, the cells are very close together, myocytes are expressing different genes due to their adult nature, and extracellular matrix exists along with mechanical stress and fluid flow. Therefore, as one can imagine, the HB-EGF signaling mechanism could vary greatly from that of the *in vitro* situation. In Chapter Four I developed a computational model to predict how far the HB-EGF signal traveled. The model is dependent on a few crucial values, however, it lead us to hypothesize that the HB-EGF ligand stays relatively localized around the point of production and does not diffuse to distant cells in the myocardium.

To determine the signaling mechanism *in vivo*, the hypertrophic response of an increase in size was once again utilized. Adult mice were first injected with Ad-HB-EGF or Ad-GFP in the left ventricle. After one week, the animal was sacrificed, the heart was fixed and stained as

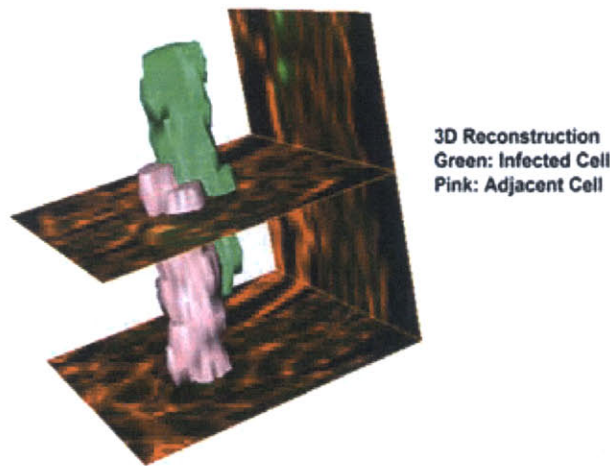


Figure 10. Three dimension reconstruction of two cardiomyocytes in the adult mouse left ventricle. The green cell is that infected with the GFP adenovirus, and the pink cell is one neighboring the virus infected cell. The x planes in the figure are vertical slices of the mouse heart, which was used to reconstruct the 3D image. The red in this plane is maleimide staining, which is an extracellular stain that serves to outline the cell for reconstruction.

outlined in the material and methods, and cardiomyocytes were identified as infected with Ad-HB-EGF or Ad-GFP due to GFP expression. Volume and cross-sectional area was measured for Ad-GFP or Ad-HB-EGF infected cells, as well as non-infected cells adjacent to the GFP expressing cell and cells remote to the site of injection or any GFP expression. Cross-sectional area was measured by evaluating the diameter of myocytes taken from slices of the entire heart. Within each slice of a mouse heart the cells are in varying orientations, therefore only cross-sectional areas that were circular were analyzed so that no discrepancies in cell orientation would skew the data. The volume of cardiomyocytes was measured with a new novel and inexpensive approach to 3D imaging. Images were taken of consecutive slices throughout the mouse myocardium in ten micron

outlined in the material and methods, and cardiomyocytes were identified as infected with Ad-HB-EGF or Ad-GFP due to GFP expression. Volume and cross-sectional area was measured for Ad-GFP or Ad-HB-EGF infected cells, as well as non-infected cells adjacent to the GFP expressing cell and cells remote to the site of injection or any GFP expression. Cross-sectional area was measured by evaluating the diameter of myocytes taken from slices of the entire heart. Within each slice of a mouse heart the cells are in varying orientations, therefore only cross-sectional areas that were circular were

intervals, and these images were registered in Matlab, and the cells were reconstructed. Figure 10 illustrates two cardiomyocytes reconstructed with this approach. Note the long rod-like dimensions of each cell.

The *in vivo* cross-sectional area and volume analysis both indicated that Ad-HB-EGF infected cells and those adjacent to them were significantly larger than remote cells and all cells in the Ad-GFP control heart (Figure 11). Because the neighboring cell hypertrophies in addition to the virus infected cell, HB-EGF signaling is no longer autocrine only like in the *in vitro* case. This suggests that *in vivo*, HB-EGF acts as a hypertrophic signal to the cells which produced the ligand and the immediately adjacent neighbors. Since the remote cells remain small, we conclude that the HB-EGF signal does not travel far, and only affects the cells adjacent to the HB-EGF source. Therefore, HB-EGF signaling *in vivo* is autocrine and local paracrine for cells in close proximity.

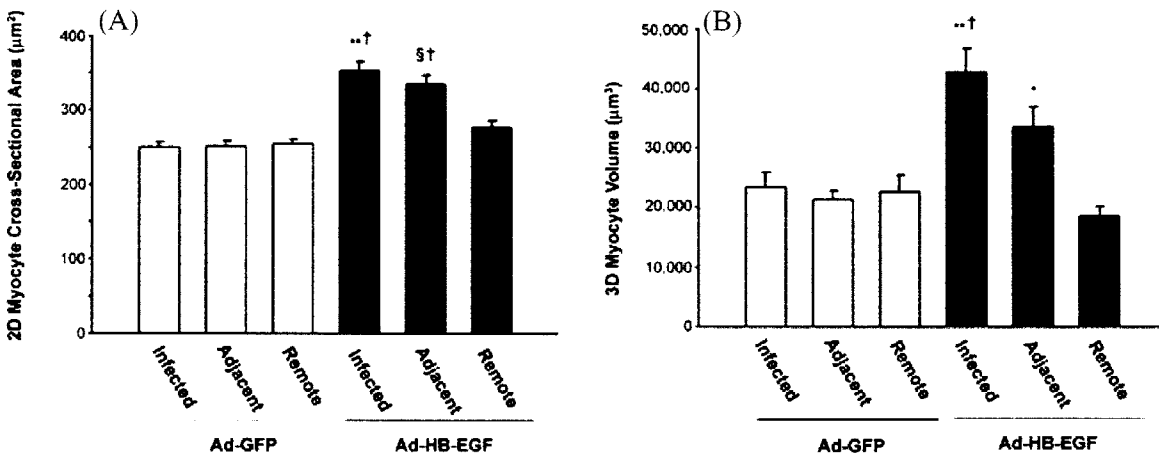
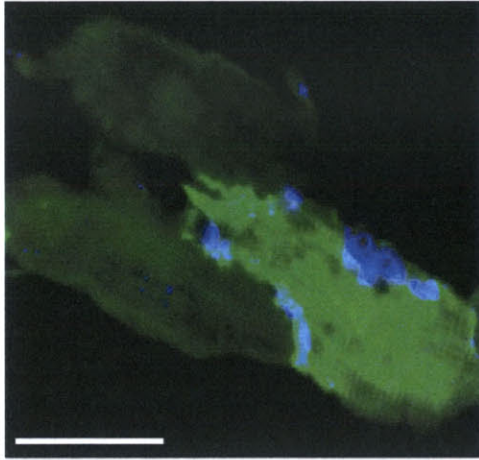


Figure 11. *In Vivo* Cardiomyocyte Cell Size (A) Two-dimensional cross-sectional area of myocytes measured from left ventricle cross sections. Virus infected cells expressing GFP were analyzed, as well as cells adjacent to the GFP expressing cells, and cells remote to the GFP expressing cell in each of the Ad-HB-EGF and Ad-GFP injected hearts. Ad-HB-EGF caused a significant increase in size (41% increase compared to Ad-GFP-infected cells, ** $P < 0.01$) and non-infected adjacent cells to Ad-HB-EGF (33% increase of Ad-GFP-adjacent cells, § $P < 0.01$) compared to remote cells. In Ad-GFP injected hearts ($n_{\text{infected}}=102$ cells, $n_{\text{adjacent}}=92$ cells, $n_{\text{remote}}=97$ cells from 5 mice), and in Ad-HB-EGF injected hearts ($n_{\text{infected}}=119$ cells, $n_{\text{adjacent}}=97$ cells, $n_{\text{remote}}=109$ cells from 7 mice). (B) Three-dimensional myocyte volume measured from left ventricle cross-sections registered in the z plane. Virus infected cells expressing GFP were analyzed, as well as cells adjacent to the GFP expressing cells, and cells remote to the GFP expressing cell in each of the Ad-HB-EGF and Ad-GFP injected hearts. Ad-HB-EGF induced hypertrophy in the infected cell and its adjacent cell only. Ad-HB-EGF cell volumes were significantly greater than Ad-GFP infected cells (** $P < 0.01$) and remote cells in the Ad-HB-EGF injected heart († $P < 0.01$). Additionally, cells adjacent to the Ad-HB-EGF cells were significantly larger than remote cells in the Ad-HB-EGF (* $P < 0.05$) injected heart. In Ad-GFP injected hearts ($n_{\text{infected}}=12$ cells, $n_{\text{adjacent}}=10$ cells, $n_{\text{remote}}=9$ cells) and in Ad-HB-EGF injected hearts ($n_{\text{infected}}=19$ cells, $n_{\text{adjacent}}=11$ cells, $n_{\text{remote}}=13$ cells).



Blue: HB-EGF

Figure 12. Immunohistochemistry of Mouse Left Ventricle Cross-sections injected with Ad-HB-EGF. Blue staining is for HB-EGF (Alexa Fluor 555) and green cells are those that have received the HB-EGF adenovirus. Blue staining is only present around the virus infected cell. Scale bar represents 20 μ m.

To visually inspect localized HB-EGF signaling in the myocardium, slices of the mouse heart were analyzed with immunohistochemistry. Figure 12 is a cross-section from a mouse heart previously injected with Ad-HB-EGF. Staining for HB-EGF in blue reveals that HB-EGF is localized around the GFP-expressing cell, which has been infected with Ad-HB-EGF.

In conclusion, HB-EGF acts as an autocrine and paracrine factor *in vivo*, but only signals to cells in close proximity of the ligand producing cell. Therefore, HB-EGF acts a local paracrine factor and autocrine factor, which is reflected in the computational model. As predicted by the model, the reason for this localization of HB-EGF signaling may be contributed to the tissue architecture, with its large density of capillaries to remove HB-EGF from the interstitial space.

Chapter Six: Ad-HB-EGF decreases Connexin43

After establishing HB-EGF as a localized growth factor in the heart, the next step was to look at the effect of local HB-EGF. Of particular interest was the gap junction protein, Connexin43, for two reasons. First, previous studies have reported decreased Connexin43 content in liver epithelial cells stimulated with EGF (Leithe 2003). Second, it is well established that in the heart, excess mechanical stress leads to cardiac hypertrophy, in which ventricular arrhythmias are more common (Volders 1998). Connexin43 is the major gap junctional protein which allows electrical coupling between cardiomyocytes, and altered Connexin43 expression can produce arrhythmogenic substrates in heart failure (Poelzing 2004). These facts hinted that HB-EGF may play a role in the progression from cardiac hypertrophy to ventricular arrhythmias by decreasing the Connexin43 content in cardiomyocytes. However, to prove exactly this would be a major undertaking, and require much more than is presented here. But, this led us to hypothesize that HB-EGF causes a decrease in Connexin43 in cardiomyocytes.

To first test this hypothesis, protein content was analyzed with western blotting of cultures of rat neonatal cardiomyocytes infected with Ad-HB-EGF, Ad-GFP, or non-infected cells. This shows that the total amount of Connexin43 was greatly reduced in cardiomyocytes over-producing HB-EGF (Ad-HB-EGF) (Figure 13A). However, in comparison to non-infected cells, cells with Ad-GFP additionally show a small decrease in Connexin43, which could be a result of the GFP protein, virus infection, or Akt/STAT3 activation. The same blot was then probed with antibodies against N-Cadherin (an intercellular adhesion protein) and actin to show equal loading of cell lysates before gel electrophoresis. Additionally, total ERK1/2 and phospho-ERK1/2 was analyzed to show activation of this kinase, which is downstream of EGFR transactivation. Figure 13A shows that phospho-ERK1/2 levels were at their highest, and therefore the EGFR pathway was activated, in Ad-HB-EGF infected cells. Ad-GFP cells showed slight activation of EGFR through phospho-ERK1/2 compared to non-infected cells, which is consistent with the slight reduction in Connexin43. Therefore, *in vitro*, Ad-HB-EGF leads to a reduction in Connexin43.

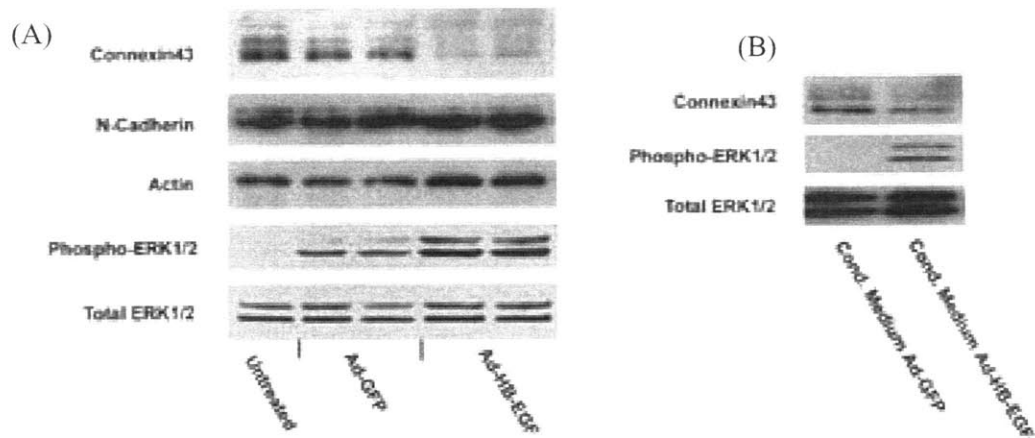


Figure 13 HB-EGF leads to a decrease in Connexin43 in rat neonatal cardiomyocytes. (A) Western blotting of cardiomyocyte cell lysates shows that Ad-HB-EGF caused a decrease in Connexin43, and activated ERK1/2. Total ERK1/2, actin, and N-Cadherin are all present in equal amounts demonstrating the equal loading of the gel. (B) Conditioned medium from Ad-HB-EGF cell lysates activated ERK1/2, but led to a modest decrease in Connexin43 *in vitro*.

Conditioned medium from Ad-GFP and Ad-HB-EGF was removed from each dish and placed on naïve cells. Western blotting of naïve cells showed no change in Connexin43, despite phospho-ERK1/2 activation (Figure 13B). This is consistent with the *in vitro* hypertrophy data which illustrated that HB-EGF acts primarily as an autocrine growth factor *in vitro*.

To confidently show that the reduction in Connexin43 is through the EGFR pathway, Connexin43 content was analyzed in the presence of the EGFR tyrosine kinase inhibitor, AG1478 (10 μ M) (Figure 14). This western blot shows that use of the EGFR inhibitor returned some content of Connexin43 to cardiomyocytes *in vitro*, however, not to the same levels of the Ad-GFP infected cells. In addition, use of the inhibitor on Ad-GFP appears to increase the amount of Connexin43 present.

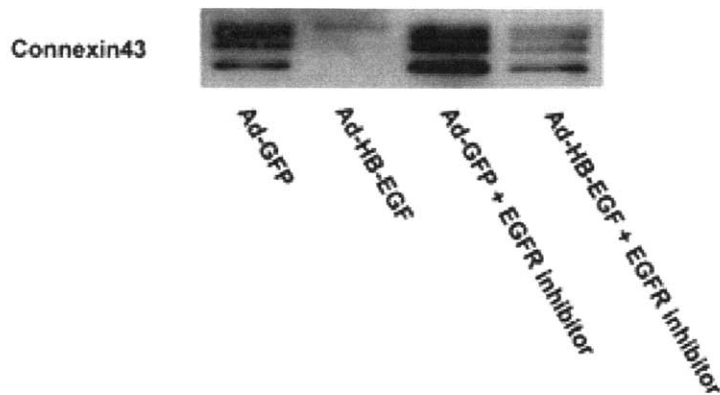


Figure 14 Connexin43 decrease due to HB-EGF happens partially through the EGFR. The EGFR tyrosine kinase inhibitor AG1478 partially abolished the reduction in Connexin43 seen in Ad-HB-EGF infected cells, suggesting that the Connexin43 decrease is linked to activation of the EGFR.

HB-EGF and activation of the EGFR led to a reduction in Connexin43 in cardiomyocytes; however, the mechanism of this decrease is unknown. Connexin43 could decrease due to a slower production rate of new Connexin43 or a faster degradation or endocytosis rate of Connexin43 that was previously present in the plasma membrane. To analyze production of new Connexin43, Northern analysis was utilized to compare the quantities of mRNA present in Ad-HB-EGF, Ad-GFP, and non-infected cardiomyocytes (Figure 15). Connexin43 mRNA levels were all relatively the same for each of the cell treatments. This suggests that HB-EGF effects Connexin43 after translation of the protein.

Eukaryotic cells utilize several pathways for degradation of proteins. Two of the major contributors to protein degradation are the proteasome and the lysosome. The lysosome is an organelle with an acidic interior full of hydrolytic enzymes that primarily degrade extracellular proteins taken up by the cell (Lodish 2004). Proteasomal degradation is most prominent in the cytosol, where the molecule ubiquitin is added to lysine side chains as a tag for the protein to be degraded. Degradation of Connexin43 gap junctions involves both the proteasome and the lysosome (Laing 1997), and EGF stimulated degradation leads to the ubiquitination and subsequent proteasomal degradation of Connexin43 in epithelial cells (Leithe 2004). However, in the case of cardiomyocytes, the ubiquitination pattern of Connexin43 yielded puzzling results for Ad-HB-EGF and Ad-GFP infected cells (Figure 16). Therefore, we found inconclusive results for the mechanism in which HB-EGF leads to a decrease of Connexin43 in Ad-HB-EGF infected cells. However, it should be noted that the lysosomal pathway for protein degradation was not analyzed.

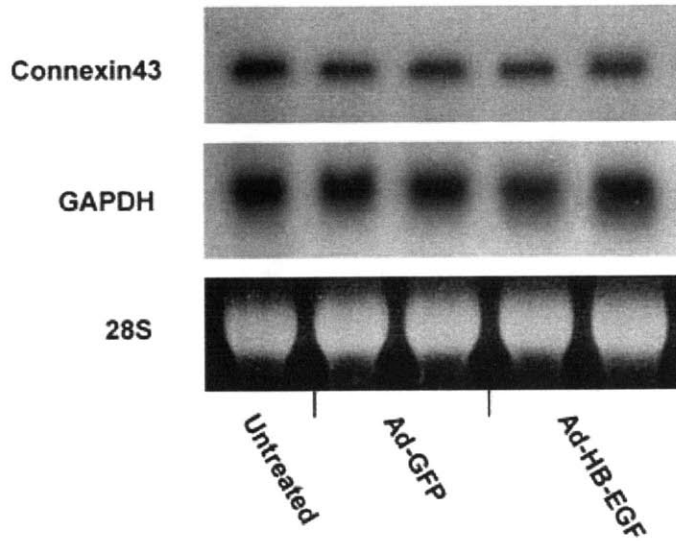


Figure 15 Ad-HB-EGF does not change mRNA levels in rat neonatal cardiomyocytes. Northern analysis for Connexin43 gene expression using a rat Cx43 cDNA probe showed equal amounts of Connexin43 mRNA in Ad-GFP, Ad-HB-EGF, and non-infected cells. This indicated that the decrease in Connexin43 is not due to a decrease in gene expression. GAPDH and 28S are shown for equal loading of the Northern blot.

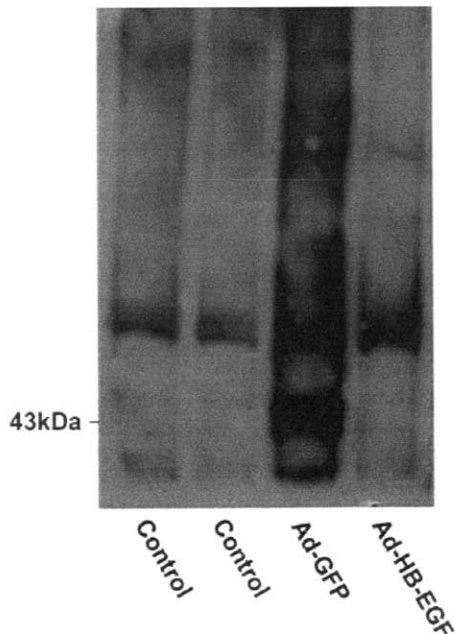


Figure 16. Ubiquitination of Connexin43. Connexin43 was immunoprecipitated from cardiomyocyte cell lysates infected with Ad-GFP, Ad-HB-EGF, and non-infected cells. Western blotting with anti-ubiquitin antibodies showed a slight increase in ubiquitinated Connexin43 in Ad-HB-EGF cells, and a large increase in Ad-GFP compared to control cells.

The next logical step in analyzing Connexin43 was to determine whether HB-EGF has the same reducing effect on Connexin43 *in vivo*. Therefore, slices from the adult mouse heart which had been previously injected with Ad-HB-EGF or Ad-GFP were stained with anti-

Connexin43 antibodies and confocal images were taken. In comparison, less positive Connexin43 staining is present in the virus infected areas of an Ad-HB-EGF injected mouse rather than an Ad-GFP mouse (Figure 17).

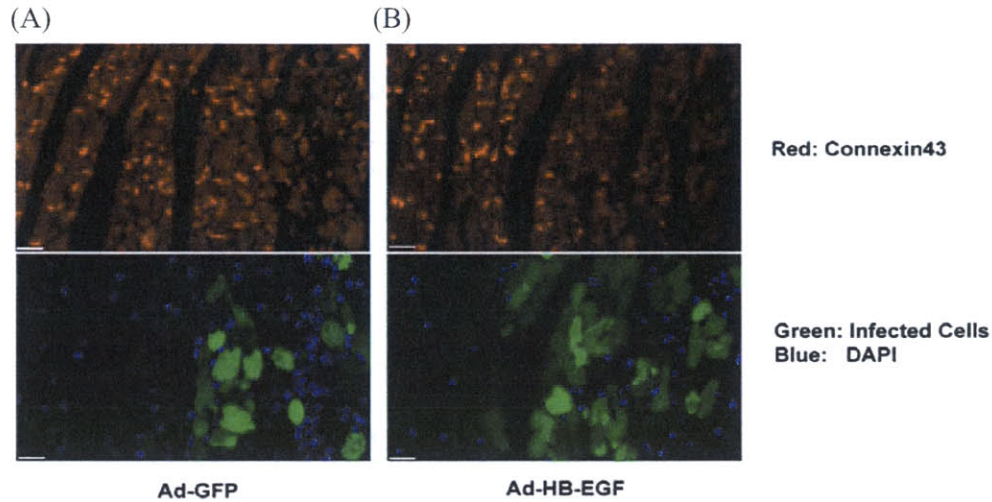


Figure 17. Fluorescent images of Connexin43 in Ad-HB-EGF and Ad-GFP injected mouse myocardium. (A) Mouse hearts injected with Ad-GFP showed equal expression of Connexin43 (top, red) in virus infected areas (bottom, green) and areas without GFP expression. The top and bottom images are the same view, with the top as the red channel showing even Connexin43 distribution across the entire picture. Blue staining is for nuclei. (B) Mouse hearts injected with Ad-HB-EGF showed less expression of Connexin43 (top, red) in areas which overlap the GFP expressing cells (green). The left part of the top image has more Connexin43 staining than the right half of the top image, demonstrating that the right half is producing HB-EGF from Ad-HB-EGF infection and has less Connexin43. Scale bars represent 20µm.

In order to quantify this observation, I wrote a program (Matlab code in Appendix A and B) to identify green areas within an image (virus infected areas), measure this area, and identify and quantify positive Connexin43 staining in this area. The program additionally identified and quantified Connexin43 in tissue within an 18 µm radius of the green tissue, referred to as the adjacent area. Additionally, confocal images were taken of areas of the myocardium with no signs of GFP expression or virus infection for comparison and normalization of the staining conditions. Figure 18 shows that the amount of Connexin 43 measured in cells infected with Ad-HB-EGF is significantly less than Ad-GFP. Connexin43 is also less in areas adjacent to Ad-HB-EGF rather than areas adjacent to Ad-GFP. This is consistent with the *in vivo* computational model prediction on the extent of HB-EGF diffusion and the *in vivo* hypertrophy data indicating hypertrophic responses only in virus infected and neighboring cells. As degradation of Cx43 may accompany structural changes with marked rearrangement of intercellular connections, we

also explored if the cell-adhesion molecule, N-cadherin, was affected by overexpression of HB-EGF. In contrast to Connexin43, there was no significant difference in total area occupied by N-cadherin immunoreactive signal in between Ad-GFP (n=19) and Ad-HB-EGF hearts (1.8 ± 0.5 -fold compared with Ad-GFP, n=17, $P=0.7$), indicating that HB-EGF has a selective effect on Connexin43.

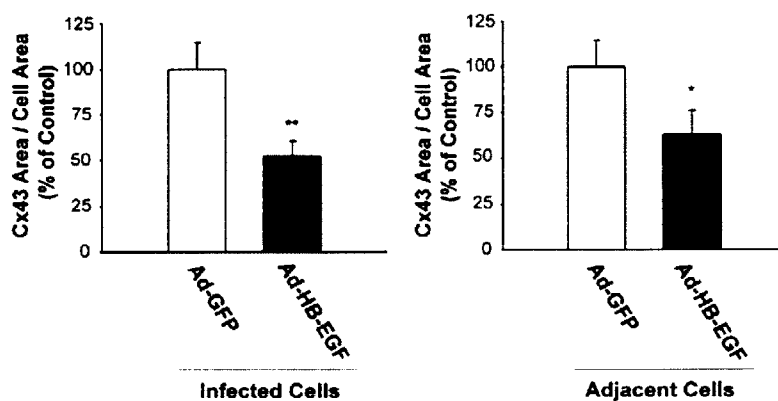


Figure 18. Quantification of Connexin43 staining *in vivo*. (A) Connexin43 is significantly reduced in cells infected with Ad-HB-EGF compared to Ad-GFP (52% decrease, $**P<0.01$). (B) Adjacent areas to the virus infected tissue (within and 18 μ m radius) showed a significant reduction in the amount of Connexin43 (37% decrease, $*P<0.05$). Connexin43 data is in Connexin43 staining area per tissue area analyzed, and these numbers were normalized with remote area data for each heart to account for staining variations from heart to heart. A total of 22 fields in 6 Ad-HB-EGF injected hearts and 19 fields in 4 Ad-GFP injected hearts were analyzed.

In conclusion to Chapter Six, HB-EGF led to a reduction in the total amount of Connexin43 in cardiomyocytes *in vivo* and *in vitro*. Consistent with the hypertrophy analysis in Chapters Three and Five, this reduction was likely the result of autocrine HB-EGF signaling *in vitro* and autocrine and local paracrine signaling *in vivo*. Although the mechanism of Connexin43 loss is unknown, it is induced, at least partially, through activation of the EGFR then post-translational modification of Connexin43.

While studying this system, we observed that exogenous, recombinant HB-EGF did not give the same experimental results in regard to Connexin 43 when compared to use of Ad-HB-EGF. Exogenous HB-EGF led to signs of hypertrophy and induced a significant increase in protein synthesis in cultures of neonatal cardiomyocytes (Figure 19). However, exogenous HB-EGF nor exogenous EGF had zero effect on the amount of Connexin43 protein present in cardiomyocyte cell lysates (Figure 20). This was unexpected, because Ad-HB-EGF causes a significant decrease in Connexin43 *in vitro*. Additionally, immunoprecipitation of Connexin43

from cell lysates, and blotting with anti-ubiquitin antibodies showed no change in the ubiquitination of Connexin43 *in vitro* (data not shown).

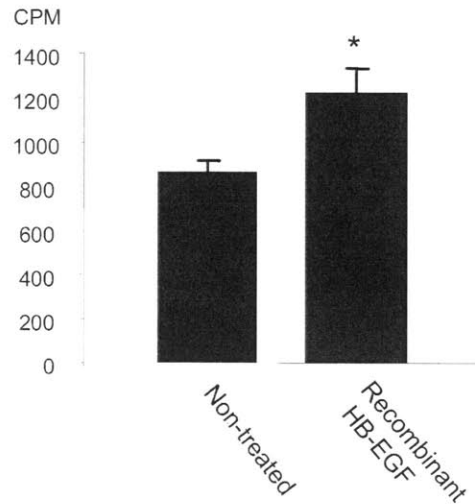


Figure 19. Protein synthesis in cardiomyocytes stimulated with exogenous HB-EGF. Exogenous, recombinant HB-EGF was added to the serum-free media of cardiomyocytes *in vitro* (10^{-8} M). The addition of HB-EGF caused a significant increase in [3 H] leucine incorporation (* $P < 0.05$) when compared to non-treated cells, $n = 6$.

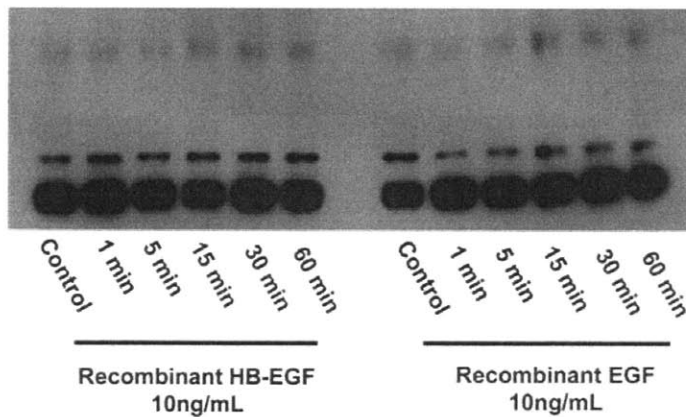


Figure 20. Exogenous, recombinant HB-EGF and EGF did not change Connexin43. Western blotting showed that HB-EGF and EGF at 10ng/mL from 1-60min stimulation time does not alter the amount of Connexin43 present in neonatal cardiomyocyte cell lysates.

Exogenous HB-EGF, purchased from Sigma Aldrich and R&D Systems are recombinant forms and have a molecular weight of around 8.3kDa. However, native HB-EGF, produced by the cell migrates as a band of 22kDa during gel electrophoresis due to heavy O-glycosylation of HB-EGF after synthesis by the cell. As Figure 2 showed in Chapter Three, the primary form of

HB-EGF present in Ad-HB-EGF cells lysates is around 22kDa, and is therefore the cleaved, glycosylated form of HB-EGF, possibly bound to heparin sulfate proteoglycans or EGFR on the cell surface. The additional bands in the western blot are assumed to be the forms of pro-HB-EGF, which exist before cleavage to form soluble HB-EGF. Therefore, the major difference between the two forms, recombinant and native, is heavy O-glycosylation in the Ad-HB-EGF produced ligand.

The different results in regards to Connexin43 reduction in Ad-HB-EGF vs. exogenous HB-EGF are puzzling, but could lead to clues about the pathway of Connexin43 degradation with further experimentation. Or, the reduction in Connexin43 could be dependent on the HB-EGF concentration. Ad-HB-EGF may be produced at a much higher concentration, or be more localized due to binding on heparin sulfate proteoglycans on the cell surface, or may be able to reach the EGF receptors more easily due to its close release from the cell surface. Additionally, the difference in HB-EGF and Ad-HB-EGF may be time. Ad-HB-EGF gives the cell prolonged HB-EGF stimulation, while exogenous HB-EGF may begin to breakdown in the media over time. However, prolonged experiments of up to 4 days exposure to exogenous HB-EGF yielded inconclusive results (data not shown). It is also possible that the sugar side chains added during glycosylation may play an unknown role in HB-EGF signaling. Another possibility is that Connexin43 reduction is only stimulated by Juxtacrine signaling, where only the pro-HB-EGF form signals to the cell, rather than the soluble form of HB-EGF. I may hypothesize many reasons for this difference in signaling, however, this puzzling phenomenon should be studied in further detail before solid conclusions can be made.

Chapter Seven: Discussion

In conclusion, this master's thesis made three major observations about cell communication and hypertrophy in the heart.

1. **HB-EGF signaling *in vitro* is autocrine only in cultures of cardiomyocytes.** Assays of cell-size and leucine incorporation show that Ad-HB-EGF induced hypertrophy only of the cells that are infected with Ad-HB-EGF, and not non-infected cells or Ad-GFP infected cells.
2. **HB-EGF signaling *in vivo* is autocrine and local paracrine only in the mouse myocardium.** This was shown experimentally and predicted by computational modeling. Experimentally, only cells infected with Ad-HB-EGF and their immediately adjacent neighbors hypertrophied, as analyzed by cell size.
3. **HB-EGF leads to a decrease in Connexin43 content *in vitro* and *in vivo*.** As analyzed by western blotting *in vitro* and immunohistochemistry, Ad-HB-EGF caused a decrease in the amount of Connexin43 present in cardiomyocytes dependent on the EGFR. The decrease was consistent with the signaling mechanism of HB-EGF, in that the virus infected cells as well as the neighboring cells had a significant reduction in Connexin43 content *in vivo*. The mechanism for Connexin43 was not elucidated, but is not thought to be through a decrease in gene expression or an increase in ubiquitination.

Therefore, we conclude that HB-EGF is designed to be a very localized remodeling factor within the heart, and only generates a cell response within a small microenvironment of signaling. This is probably due to the structure of the myocardium, with several capillaries surrounding each cardiomyocyte serving as a sink to signaling molecules, removing them from the system before they can diffuse several cells away. Additionally, this may be due to the large size of soluble HB-EGF (22kDa, glycosylated), and the multitude of heparin sulfate proteoglycans present in the extracellular matrix and on the cell surface for HB-EGF to bind. The small microenvironment of HB-EGF signaling leads to a small area with a reduction of Connexin43. This reduction *in vitro* is very drastic, with a 73% reduction in Connexin43 (Figure 13A, Figure 14). However, *in vivo* this reduction is not as pronounced, with approximately a 50% reduction in Connexin43 staining. Connexin channels consist of two units, one from each cell, which dock together to form one channel. Two cells that are electrically coupled with Connexin43 channels each donate one hemichannel to form a complete Connexin43 gap junction. Therefore, it could be possible that

the 50% reduction *in vivo* is due to contributions from neighboring cells, therefore increasing the number of channels in the virus infected cells.

Not only is the data significant in this analysis, but also the experimental techniques utilized here. We were able to take advantage of non-uniform gene transfer in the myocardium, which is normally considered a pitfall of traditional gene therapy. Additionally, the three-dimensional imaging approach is a new and inexpensive method for reconstruction of tissue. This technique requires only a standard fluorescent microscope, in which many images of vertical slices of the tissue are taken, and a computer program in Matlab is used to register the images and reconstruct the image in three dimensions. The major drawback to this approach is the imaging time required, and the poor resolution in the z-direction (10 μm spacing between vertical images). This resolution could be easily improved by taking smaller slices of the tissue, however, this increases the imaging time required. This imaging approach may not be suitable for all tissue types. In the myocardium, cardiomyocytes are long and rod-like in shape; therefore several tissue cross-sections cover the length of the cells. Tissues composed of cells spherical or square in shape might not provide good enough resolution in the z-direction to make accurate measurements of individual cell volume.

As with every experiment, this study does have its limitations. In the *in vitro* analysis, all cells used for experiments are neonatal cardiomyocytes isolated from rats 1 to 3 days old. The gene expression pattern is obviously different in neonatal cells when compared to adult cardiomyocytes. This could lead to inherent differences in results between the adult and neonatal experiments. Cardiomyocytes do not divide much after birth, therefore a stable culture of cells is never achieved. Cultured adult myocytes are fragile and live approximately 24 hours, while the neonatal cells are more viable in cell culture, living 5-6 days on average. Additionally, during isolation of cardiomyocytes, care is taken to remove cardiac fibroblasts. However, it is possible that some *in vitro* experiments had varying amount of fibroblasts in the cell culture dishes. Visual inspection was used to control for fibroblast growth. Since cardiomyocytes do not divide after becoming plated, any increase in cell density over time was expected to be fibroblasts, and the experiment was therefore terminated.

An additional consideration is that Ad-GFP caused a slight hypertrophic response in cardiomyocytes when compared to cells that have not been infected with an adenovirus. However, Ad-HB-EGF causes a hypertrophic response significantly greater than Ad-GFP; therefore, Ad-GFP still serves as a sufficient control for these experiments. Ad-GFP showing slight hypertrophy is illustrated through a small increase in cell size *in vitro* and *in vivo*, and slight phospho-ERK activation, and slight Connexin43 decrease. As mentioned in Chapter Four,

the adenovirus protein E4 has been reported to phosphorylate the kinase Akt, which may contribute to hypertrophy in cardiomyocytes. In hindsight, a better virus design might have been to alter or remove the E4 domain from the Ad-HB-EGF and Ad-GFP adenoviruses, or use an additional control of an empty viral vector. In addition, previous studies have shown that transgenic expression of GFP can lead to dilated cardiomyopathy (Huang 2000). Therefore, it is possible that GFP may lead to some of the hypertrophic characteristics demonstrated in cells infected with Ad-GFP compared to non-infected cells.

The mechanism in which HB-EGF leads to a decrease in Connexin43 was never elucidated. Northern analysis (Figure 15) to look at the levels of gene expression and western blot analysis of ubiquitinated Connexin43 (Figure 16) to analyze degradation through the proteasome pathway gave inconclusive results. Both assays suggested that neither mechanism were involved in the decrease of Connexin43. However, gene expression and degradation can be a very transient process and it is possible that these assays were simply not performed at the appropriate points in time. In addition, the lysosomal pathway for protein degradation was never analyzed, and therefore it could also be the main contributor to the decrease in Connexin43.

Finally, as with any computational model, the one presented here has many limitations and is based on assumptions made. The model assumes a two-dimensional geometry due to the long rod-like dimensions of a cardiomyocyte, and therefore does not analyze diffusion of HB-EGF between the intercalated discs. Additionally, most of the modeling parameters are best estimates and many are based on the well-studied EGF, rather than HB-EGF. Unfortunately, one of the most important values governing the extent of HB-EGF diffusion in the computational model was a value that has not been measured for hardly any growth factors, the mass transfer coefficient through the capillary walls. The mechanism for this transport is even unknown; therefore a best guess at its value was utilized. At lower value of the mass transfer coefficient, HB-EGF was predicted to diffuse past six or more cells. This length of diffusion becomes close to the length scale of a cardiomyocyte, and therefore the two-dimensional model begins to break down because diffusion is likely to occur through the intercalated discs. A three-dimensional model would be more apt to analyze this situation.

One final issue to discuss is the opposing data in the literature which indicate that other hypertrophic molecules upregulate the amount of Connexin43 in the myocardium. In the early phase of cardiac hypertrophy, cardiac gap junctions are upregulated, while gap junctions are subsequently downregulated in the progression from hypertrophy to cardiac failure (Saffitz 2004). *In vitro*, long term exposure to cAMP (Darrow 1996), angiotensin II (Dodge 1998), endothelin-1 (Polontchouk 2001), VEGF and TGF- β (Pimental 2002), as well as brief periods of pulsatile

stretch (Zhuang 2000) increase Connexin43 expression in cardiomyocytes. These signaling molecules are likely regulated by mechanical stretch, in that stretch activates numerous pathways in cardiac myocytes and induces the release of angiotensin II, endothelin-1, VEGF, and TGF- β (Saffitz 2004). However, stretch additionally leads to the endothelin-1 dependent cleavage of pro-HB-EGF (Asakura 2002), and as we have shown here, HB-EGF leads to a decrease in Connexin43. This is a puzzling phenomenon, in that stretch produces factors that upregulate and downregulate Connexin43, possibly to balance the number of gap junctions present in a cardiomyocytes or to provide a time course in which Connexin43 is upregulated then subsequently downregulated. HB-EGF may link previous research showing that JNK leads to a severe decrease in Connexin43 expression (Petrich 2002), and as we have shown here, Ad-HB-EGF leads to activation of JNK. Therefore, HB-EGF may be a key molecule that downregulates Connexin43 channels in the later phase of cardiac hypertrophy.

Despite any limitation or assumptions made in this thesis, I feel that the data confidently proves that HB-EGF is a localized mediator of cell communication in the heart and leads to a significant reduction in Connexin43 *in vitro* and *in vivo*.

Chapter Eight: Future Directions

This project opens many doors into further study of this system. The next logical step would be to determine the mechanism for Connexin43 decrease in the cell and to study if this decrease changes the electrical properties of the heart.

In the modeling section, future directions would be to construct a more inclusive model of EGFR binding and trafficking, and extracellular matrix and heparan sulfate proteoglycan binding. Accumulating more quantitative data on parameters important to the mathematical model, such as the mechanism and rate of HB-EGF transfer through the capillary walls; the production rate of HB-EGF in response to mechanical stress; the number of EGF receptors on the surface of an adult myocyte; the number of binding sites for HB-EGF within the extracellular matrix; and the number of binding sites for HB-EGF present on the cell surface due to heparan sulfate proteoglycans will be required. Using this data, the model could be significantly improved and used to predict transient HB-EGF concentration rather than only at steady-state.

Of additional future interest is to study HB-EGF signaling and Connexin43 dynamics on a subcellular level, and to determine if this system has the ability to promote highly localized tissue remodeling in the myocardium in response to small subcellular mechanical stresses. .

Acknowledgements

I would like to thank my advisors, Douglas Lauffenburger and Richard Lee and my research team in working on this paper and contributing time and data to this project, including Jun Yoshioka, Hayden Huang, Scott Perkins, Francisco Cruz, and Catherine MacGillivray. I would additionally like to thank Mihaela Cupesi and Jeremy D. Sylvan for their technical assistance. This work was supported by grants from the National Institutes of Health (to R.T.L., H.H., and D.A.L.), National Science Foundation (to R.N.P.), and the American Association of University Women (to R.N.P.).

References

- Abdelmohsen K (2003), Berber PA, Montfort CV, Sies H, Klotz L. Epidermal growth factor receptor is a common mediator of quinon-induced signaling leading to phosphorylation of connexin-43. *J Biol Chem.* 278:38360-7.
- Abraham JA (1993), Damm D, Bajardi A, Miller J, Klagsbrn M, Ezekowitz, RAB. Heparin-binding EGF-like growth factor: characterization of rat and mouse cDNA clones, protein domain conservations across species, and transcript expression in tissues. *Biochem Biophys Res Commun.* 190:125-33.
- Anderson HDI (2004), Wang F, Gardner DG. Role of the epidermal growth factor receptor in signaling strain-dependent activation of the brain natriuretic peptide gene. *J Biol Chem.* 279:9287-97.
- Asakura M (2002), Kitakaze M, Takashima S, Liao Y, Ishikura F, Yoshinaka T, Ohmoto H, Node K, Yoshino K, Ishiguro H, Asanuma H, Sanada S, Matsumura Y, Takeda H, Beppu S, Tada M, Hori M, Higashiyama S. Cardiac hypertrophy is inhibited by antagonism of ADAM12 processing of HB-EGF: metalloproteinase inhibitors as a new therapy. *Nature Medicine.* 8:35-40.
- Bolamba D (2002), Floyd AA, McGone JJ, Lee VH. Epidermal growth factor enhances expression of connexin 43 protein in cultured porcine preantral follicles. *Biol Reprod.* 67:154-60.
- Chien KR (1999). *Molecular Basis of Cardiovascular Disease.* Philadelphia: W.B. Saunders Co.
- Darrow BJ (1996) Fast VG, Kleber AG, Beyer EC, Saffitz JE. Functional and structural assessment of intercellular communication: increased conduction velocity and enhanced connexin expression in dibutyryl cAMP treated cultured cardiac myocytes. *Circ Res.* 79:174-183.
- DeWitt AE (2001), Dong JY, Wiley HS, Lauffenburger DA. Quantitative analysis of the EGF receptor autocrine system reveals cryptic regulation of cell response by ligand capture. *J Cell Sci.* 114:2301-13.
- Dodge SM (1998), Beardslee MA, Darrow BJ, Green KG, Beyer EC, Saffitz JE. Effects of angiotensin II on expression of the gap junction channel protein connexin43 in neonatal rat ventricular myocytes. *J Am Coll Cardiol.* 32:800-807.
- Dowd CJ (1999), Cooney CL, Nugent MA. Heparan sulfate mediates bFGF transport through basement membrane by diffusion with rapid reversible binding. *J Biol Chem.* 274:5236-44.
- Elenius K (1997), Subroto P, Allison G, Sun J, Klagsbrun M. Activation of HER4 by heparin-binding EGF-like growth factor stimulates chemotaxis but not proliferation. *The EMBO Journal.* 16:1268-78.
- Huang, WY (2000), Aramburu J, Douglas PS, Izumo S. Transgenic expression of green fluorescence protein can cause dilated cardiomyopathy. *Nat Med.* 6:482-3.
- Higashiyama S (1991), Abraham JA, Miller J, Fiddes JC, Klagsbrun K. A heparin-binding growth factor secreted by macrophage-like cells that is related to EGF. *Science.* 251:936-39.

- Higashiyama S (1993), Abraham JA, Klagsbrun M. Heparin-binding EGF-like growth factor stimulation of smooth muscle cell migration: dependence on interactions with cell surface heparan sulfate. *J Cell Biol.* 122:933-40.
- Kostin S (2003), Rieger M, Dammer S, Hein S, Richter M, Klovekorn WP, Bauer EP, Schaper. Gap junction remodeling and altered connexin43 expression in the failing human heart. *Mol Cell Biochem.* 242:135-44.
- Laing JG (1997), Tadros PN, Westphale EM, Beyer EC. Degradation of connexin43 gap junctions involves both the proteasome and the lysosome. *Exp Cell Res.* 235:482-92.
- Lau AF (1992), Kanemitsu MY, Kurata WE, Danesh S, Boynton AL. Epidermal Growth Factor Disrupts Gap-Junctional Communication and Induces Phosphorylation of Connexin43 on Serine. *Mol Biol Cell.* 3:865-74.
- Lauffenburger DA (1998), Oehrtman GT, Walker L, Wiley HS. Real-time quantitative measurement of autocrine ligand binding indicates that autocrine loops are spatially localized. *Proc Natl Acad Sci U SA* 95:15368-73.
- Leithe E (2004), Rivedal E. Epidermal growth factor regulates ubiquitination, internalization and proteasome-dependent degradation of connexin43. *J Cell Sci.* 117:1211-20.
- Lindsey ML (2003), Yoshioka J, MacGillivray C, Muangman S, Gannon J, Cerghese A, Aikawa M, Libby P, Kranc SM, Lee RT. Effect of a cleavage-resistant collagen mutation on left ventricular remodeling. *Circ Res.* 93:238-45.
- Lodish H (2004), Berk A, Matsudaira P, Kaiser C, Krieger M, Scott M, Zipursky SL, Darnell J. *Molecular Cell Biology*. New York: W.H. Freeman and Co. p535.
- Massague J (1993), Pandiella A. Membrane-anchored growth factors. *Annu Rev Biochem* 62:515-41.
- Miyamoto T (2004), Takeishi Y, Takahashi H, Shishido T, Arimoto T, Tomoike H, Kubota I. Activation of distinct signal transduction pathways in hypertrophied hearts by pressure and volume overload. *Basic Res Cardiol.* 99(5):328-37.
- Peters NS (1996). New insights into myocardial arrhythmogenesis: distribution of gap-junctional coupling in normal, ischaemic and hypertrophied human hearts. *Clin Sci (Lond)* 90:447-52.
- Petrich BG (2004), Gong X, Lerner DL, Wang X, Brown JH, Saffitz JE, Wang Y. C-Jun N-terminal kinase activation mediates downregulation of connexin43 in cardiomyocytes. *Circ Res.* 91:640-7.
- Pimentel RC, Yamada KA, Kleber AG, Saffitz JE. Autocrine regulation of myocytes Cs43 expression by VEGF. *Circ Res.* 90:671-77.
- Poelzing S (2004), Rosenbaum DS. Altered connexin43 expression produces arrhythmias substrate in heart failure. *Am J Physiol Heart Circ Physiol.* 287:H1762-70.

- Polontchouk L (2001), Ebel B, Jackels M, Dhein S. Chronic effects of endothelin 1 and angiotensin II on gap junctions and intercellular communication in cardiac cells. *FASEB J*. 16(1):87-9.
- Rippe B (2002), Rosengren BI, Carlsson O, Venturoli D. Transendothelial transport: the vesicle controversy. *J Vasc Res*. 39:375-90.
- Rivedal E (2001), Opsahl H. Role of PKC and MAP kinase in EGF- and TPA-induced connexin43 phosphorylation and inhibition of gap junction intercellular communication in rat liver epithelial cells. *Carcinogenesis*. 22:1543-50.
- Sadoshima J (1997), Izumo S. The cellular and molecular response of cardiac myocytes to mechanical stress. *Annu Rev Physiol*. 59:551-71.
- Saffitz JE (2004), Kleber AG. Effects of mechanical forces and mediators of hypertrophy on remodeling of gap junctions in the heart. *Circ Res*. 94:585-591.
- Sahin U (2004), Weskamp G, Kelly K, Zhou M, Higashiyama S, Peschon J, Hartmann D, Saftig P, Blobel, CP. Distinct roles for ADAM10 and ADAM17 in ectodomain shedding of six EGFR ligands. *J Cell Biol*. 164:769-79.
- Shah BH (2003), Catt KJ. A central role of EGF receptor transactivation in angiotensin II-induced cardiac hypertrophy. *Trends Pharmacol Sci*. 24:239-44.
- Sharan M (2002), Popel AS. A compartmental model for oxygen transport in brain microcirculation in the presence of blood substitutes. *J Theor Biol*. 216:479-500.
- Shvartsman SY (2001), Wiley HS, Deen WM, Lauffenburger DA. Spatial range of autocrine signaling: modeling and computational analysis. *Biophys J* 81:1854-67.
- Tagarakis CVM (2000), Bloch W, Hartmann G, Hollmann W, Addicks K. Testosterone-propionate impairs the response of the cardiac capillary bed to exercise. *Med Sci Sports Exerc*. 32:946-53.
- Thorne RG (2004), Hrabetova S, Nicholson C. Diffusion of epidermal growth factor in rat brain extracellular space measured by integrative optical imaging. *J Neurophysiol*. 92: 3471-81.
- Tompkins RG (1991). Quantitative analysis of blood vessel permeability of squirrel monkeys. *Am J Physiol*. 260:H1194-204.
- Ueki T (2001), Fujita M, Sato K, Asai K, Yamada K, Kato T. Epidermal growth factor down-regulates connexin-43 expression in cultured rat cortical astrocytes. *Neurosci Lett*. 313: 53-6.
- Volders PGA (1998), Sipido KR, Vos MA, Kulcsar A, Verduyn SC, Wellens HJJ. Arrhythmogenesis in dogs with chronic complete atrioventricular block and acquired torsade de pointes. *Circulation*. 98:1136-47.
- Warn-Cramer BJ (1998), Cottrell GT, Burt JM, Lau AF. Regulation of connexin-43 gap junctional intercellular communication by mitogen-activated protein kinase. *J Biol Chem*. 273:9188-96.

Yoshioka J (2004), Schulze C, Cupesi M, Sylvan J, MacGillivray C, Gannon J, Huang H, Lee RT. Thioredoxin-interacting protein controls cardiac hypertrophy through regulation of thioredoxin activity. *Circulation*. 109:2581-86.

Zhang F (2004), Cheng J, Hackett NR, Lam G, Shido K, Pergolizzi R, Jin DK, Crystal RG, Rafii S. Adenovirus E4 gene promotes selective endothelial cell survival and angiogenesis via activation of the vascular endothelial-cadherin/Akt signaling pathway. *J Biol Chem*. 279(12):11760-6.

Zhuang J (2000), Yamada KA, Saffitz JE, Kleber AG. Pulsatile stretch remodels cell-to-cell communication in cultured myocytes. *Circ Res*. 87:316-22.

Appendix

Appendix A – Matlab code which calculates the Connexin43/Cadherin Staining through a blue channel within the green areas (Ad-GFP/Ad-HB-EGF infected cells) or in an 18 μ m radius of the virus infected cell (neighboring/adjacent cells)

MATLAB CODE

```
%Robin Prince 9.27.04
%Function to calculate the area of Cx43 or Cadherin staining to the area of
%interest for green cells

function [Out]=robin_g_varyblue_halo(directory)
cd(directory); %all images must be in one file and this creates a directory of those images
dr=dir('*.*tif');
dr={dr.name};
names=dr'
n=0;
n=size(dr,2); %n is the number of images in the folder
Out=zeros(n,11);

for i=1:n;
figure(1), h=imread(dr{i}); %reads in image
[A,r]=imcrop(h); %crops image to user specifications (around green area)
figure(2), imshow(A), title('Cropped Image'); %shows cropped image
g=A(:,2); %green channel of image only
h=fspecial('disk',5); %filter specifications
gf=imfilter(g,h); %filters green channel image
gf=imfilter(gf,h); %repeat
gf=imfilter(gf,h); %repeat
%figure(2), imshow(gf), title('Blurred Image'); %shows filtered image
gfbw=im2bw(gf,.15); %turns green filtered image to B&W only
gfbwstrel=gfbw;
blue=A(:,3); %blue channel of cropped image
%figure(4), imshow(A(:,3)), title('Blue Image'); %shows cropped image
bluebw=im2bw(blue,.45); %turns blue only image to B&W
%figure(5), imshow(bluebw), title('Blue to B&W'); %shows B&@ image
overlay=gfbwstrel.*bluebw; %new image of only blue where it overlaps green area in B&@
%figure(6), imshow(overlay), title('Overlapping Area of Green and Blue'); %shows overlap
image

%STATISTICS
dbw=bwlabel(gfbwstrel); %labels portions of B&W image
stats=regionprops(dbw); %gets statistics on items in image
areablue0=0;
areablue1=0;
areablue2=0;
areablue3=0;
areablue4=0;
areablue5=0;
areablue6=0;
```

```

areagreen=0;
bluesum0=0;
bluesum1=0;
bluesum2=0;
bluesum3=0;
bluesum4=0;
bluesum5=0;
bluesum6=0;
Ratio0=0;
Ratio1=0;
Ratio2=0;
Ratio3=0;
Ratio4=0;
Ratio5=0;
Ratio6=0;
greensum=0;

m=0;
for j=1:size(stats,1)
    if stats(j).Area>10
        m=m+1;
        areagreen(m,:)=stats(j).Area;
    end
end
%loop puts all grecn areas greater than 10 pixels in a matrix

overlay2=bwlabel(overlay); %makes B&W only image of the overlay
stats=regionprops(overlay2); %gets statistics on overlay image
m=0;
p=0;
q=0;
s=0;
t=0;
u=0;
v=0;
for k=1:size(stats,1)
    if stats(k).Area>0
        m=m+1;
        arcabluc0(m,:)=stats(k).Area;
    end
    if stats(k).Area>1
        p=p+1;
        areablue1(p,:)=stats(k).Area;
    end
    if stats(k).Area>2
        q=q+1;
        areablue2(q,:)=stats(k).Area;
    end
    if stats(k).Area>3
        s=s+1;
        areablue3(s,:)=stats(k).Area;
    end
end

```

```

end
if stats(k).Area>4
    t=t+1;
    areablue4(t,:)=stats(k).Area;
end
if stats(k).Area>5
    u=u+1;
    areablue5(u,:)=stats(k).Area;
end
if stats(k).Area>6
    v=v+1;
    areablue6(v,:)=stats(k).Area;
end
end
end
%this loop sums up all areas of connexin or cadherin (blue) that overlap
%the green areas in a matrix if their area is greater than 0,1,2,3,4,5,6,

    bluesum0=sum(areablue0,1); %sum of all blue area overlapping green area than is greater
than 0 pixels
    bluesum1=sum(areablue1,1); %sum of all blue area overlapping green area than is greater
than 1 pixels
    bluesum2=sum(areablue2,1); %sum of all blue area overlapping green area than is greater
than 2 pixels
    bluesum3=sum(areablue3,1); %sum of all blue area overlapping green area than is
greater than 3 pixels
    bluesum4=sum(areablue4,1); %sum of all blue area overlapping green area than is
greater than 4 pixels
    bluesum5=sum(areablue5,1); %sum of all blue area overlapping green area than is
greater than 5 pixels
    bluesum6=sum(areablue6,1); %sum of all blue area overlapping green area than is
greater than 6 pixels
greensum=sum(areagreen,1); %sums up all the green area
Ratio0 = bluesum0/greensum; %calculates the ratio of blue area to green area for each pixel
restriction
Ratio1 = bluesum1/greensum;
Ratio2 = bluesum2/greensum;
Ratio3 = bluesum3/greensum;
Ratio4 = bluesum4/greensum;
Ratio5 = bluesum5/greensum;
Ratio6 = bluesum6/greensum;

M=zeros(size(A));
e=im2bw(g,2);
M(:,1)=e;
M(:,2)=gfbwstrel;
M(:,3)=bluebw;
figure(7), imshow(M), title('To compare original green area to blurred area') %shows total pic

```

```

%Make Halo Around Green Cells

```

```

Halo_Area=0;
Blue_Halo_Sum_4=0;
Blue_Halo_Sum_5=0;
Blue_Halo_Sum_6=0;
Ratio_Halo_4=0;
Ratio_Halo_5=0;
Ratio_Halo_6=0;
areabluehalo4=0;
areabluehalo5=0;
areabluehalo6=0;

radius=40;
SEdisk=STREL('disk',radius);
D=imdilate(gfbwstrel,SEdisk); %dilates the green area previously by 40 pixels (18um)
%figure(8), imshow(D) %shows strel
Halo=D-gfbwstrel; %subtracts the original green area from the dilated area to give a 'halo'
around green
Blue_Halo=Halo.*bluebw; %image of blue staining only in halo (neighboring/adjacent cells)
%figure(9), imshow(Blue_Halo) %shows blue area in halo

RESULT=zeros(size(A));
RESULT(:,1)=Halo;
RESULT(:,3)=Blue_Halo;
figure(10), imshow(RERESULT) %shows final image

Hbw=bwlabel(Halo); %labels blue areas in halo
stats_halo=regionprops(Hbw); %gets statistics on blue areas in halo
figure(20), imshow(Hbw)

y=0;
m=0;
%Calculate Area of Halo
for y=1:size(stats_halo,1)
    if stats_halo(y).Area>10
        m=m+1;
        areahalo(m,:)=stats_halo(y).Area;
    end
end
end
%puts all halos which have areas greater than 10 pixels in a matrix

BHbw2=bwlabel(Blue_Halo); %labels blue images in halo
stats_halo=regionprops(BHbw2); %gets statistics on blue images in halo
z=0;
m=0;
p=0;
q=0;
%Calculate area of Blue in Halo for areas clusters from 4-6
for z=1:size(stats_halo,1)
    if stats_halo(z).Area>4
        m=m+1;

```

```

        areabluehalo4(m,:)=stats_halo(z).Area;
    end
    if stats_halo(z).Area>5
        p=p+1;
        areabluehalo5(p,:)=stats_halo(z).Area;
    end
    if stats_halo(z).Area>6
        q=q+1;
        areabluchalo6(q,:)=stats_halo(z).Area;
    end
end
end
%this loop puts all blue staining greater than 4,5,and 6 pixels in one
%matrix (could be 0-6 as before, but found 4 and greater to be most
%efficient

Halo_Area=sum(areahalo,1) %sums up total halo area
Blue_Halo_Sum_4=sum(areabluehalo4,1); %sums up blue staining in halo with areas greater
than 4 pixels
Blue_Halo_Sum_5=sum(areabluehalo5,1); %sums up blue staining in halo with areas greater
than 4 pixels5
Blue_Halo_Sum_6=sum(areabluehalo6,1); %sums up blue staining in halo with areas greater
than 6 pixels
Ratio_Halo_4=Blue_Halo_Sum_4/Halo_Area; %ratio of blue staining in halo to halo area for
pixel restriction of 4
Ratio_Halo_5=Blue_Halo_Sum_5/Halo_Area;
Ratio_Halo_6=Blue_Halo_Sum_6/Halo_Area;

Q=input('Do You Want to Use the Neighboring Cell Data (1=Yes, 0=No)')
%sometimes halo area in messy depending on how the image is cropped and
%what the green staining looks like, this allows the user to note whether
%or not he or she would like to use the data during analysis

Out(i,:)= [Ratio0,Ratio1,Ratio2,Ratio3,Ratio4,Ratio5,Ratio6, Ratio_Halo_4, Ratio_Halo_5,
Ratio_Halo_6,Q];
%puts all relevant information the user will need in the matrix out

end
csvwrite('greendata.csv',Out); %writes the total matrix out in a .csv file to be opened in excel

```

Appendix B

Appendix B – Matlab code which calculates the Connexin43/Cadherin staining through a blue channel for remote area images with no blue staining. This program allows the user to select the portion of the image to be analyzed and calculates amount of Connexin43/Cadherin area, per selection area (or tissue area).

MATLAB CODE:

```
%Robin Prince 10-4-04
%Program to find the Cx43 area around NON-GREEN CELLS
%NOTE: for non-green cclls ONLY!

function [Out_ng]=robinng(directory)

%Making a directory
cd(directory); %puts all .tif files from one folder into a directory
dr=dir('* .tif')
dr={dr.name}
names=dr'
n=size(dr,2) %n is the number of images in the folder
Out=zeros(n,7);

%loop to call up filenames from directory
for i=1:n;
arcablue=0;
bluesum=0;
box=0;
h=imread(dr{i});
[A,r]=imcrop(h); %allows user to crop image to specifications
figure(1), imshow(A), title('Cropped Image') %shows cropped image
blue=A(:,:,3); %blue channel only from cropped image
figure(2), imshow(blue),title('Blue Image'); %shows blue only image
bluebw=im2bw(blue,45); %changes blue to B&W only
figure(3), imshow(bluebw), title('Blue Transformed to B&W'); %shows B&W image
S=bwlabel(bluebw); %labels the B&W image
stats=regionprops(S); %gets stats on B&W image

%loop to add blue areas in a matrix
arcablue0=0;
areablue1=0;
areablue2=0;
areablue3=0;
areablue4=0;
areablue5=0;
areablue6=0;
arcagrecn=0;
bluesum0=0;
bluesum1=0;
bluesum2=0;
bluesum3=0;
bluesum4=0;
```

```

bluesum5=0;
bluesum6=0;
Ratio0=0;
Ratio1=0;
Ratio2=0;
Ratio3=0;
Ratio4=0;
Ratio5=0;
Ratio6=0;
box=0

m=0;
p=0;
q=0;
s=0;
t=0;
u=0;
v=0;

for k=1:size(stats,1)
    if stats(k).Area>0
        m=m+1;
        areablue0(m,:)=stats(k).Area;
    end
    if stats(k).Area>1
        p=p+1;
        areablue1(p,:)=stats(k).Area;
    end
    if stats(k).Area>2
        q=q+1;
        areablue2(q,:)=stats(k).Area;
    end
    if stats(k).Area>3
        s=s+1;
        areablue3(s,:)=stats(k).Area;
    end
    if stats(k).Area>4
        t=t+1;
        areablue4(t,:)=stats(k).Area;
    end
    if stats(k).Area>5
        u=u+1;
        areabluc5(u,:)=stats(k).Area;
    end
    if stats(k).Area>6
        v=v+1;
        areabluc6(v,:)=stats(k).Area;
    end
end
end
%this loop puts all blue features of the picture into a matrix if they are
%greater than 0,1,2,3,4,5,or 5 pixels in area (as indicated)

```

```

bluesum0=sum(areablue0,1); %sums up all blue areas greater than 0 pixels
bluesum1=sum(areablue1,1); %sums up all blue areas greater than 1 pixels
bluesum2=sum(areablue2,1); %sums up all blue areas greater than 2 pixels
bluesum3=sum(areablue3,1); %sums up all blue areas greater than 3 pixels
bluesum4=sum(areablue4,1); %sums up all blue areas greater than 4 pixels
bluesum5=sum(areablue5,1); %sums up all blue areas greater than 5 pixels
bluesum6=sum(areablue6,1); %sums up all blue areas greater than 6 pixels
box=r(3)*r(4); %box = size of cropped image
%NOTE: DO NOT CROP OUTSIDE THE IMAGE BOUNDARIES, OR THIS WILL
CALCULATE
%AREA OUTSIDE OF IMAGE

Ratio0=bluesum0/box; %calculates ratio of blue area to total areas selected in cropping for pixels
restiction of >0
Ratio1=bluesum1/box;
Ratio2=bluesum2/box;
Ratio3=bluesum3/box;
Ratio4=bluesum4/box;
Ratio5=bluesum5/box;
Ratio6=bluesum6/box;

Out_ng(i,:)= [Ratio0, Ratio1, Ratio2, Ratio3, Ratio4, Ratio5, Ratio6];
%puts all relevant results in a matrix
end
csvwrite('nongreendata.csv', Out_ng); %writes data to a .csv file, which can be opened in Excel

```